Inorg. Chem. **2004**, *43*, 5053–5068

Synthesis and Characterization of a New Family of Bi-, Tri-, Tetra-, and Pentanuclear Ferric Complexes

Colette Boskovic,*,† Andreas Sieber,† Grégory Chaboussant,† Hans U. GÜdel,† JÜrgen Ensling,‡ Wolfgang Wernsdorfer,§ Antonia Neels,|| Gael Labat,|| Helen Stoeckli-Evans,|| and Stefan Janssen⊥

Departement für Chemie und Biochemie, Universität Bern, Freiestrasse 3, Bern CH-3012, Switzerland, Institut für Anorganische Chemie und Analytische Chemie, Johannes Gutenberg Universität, Staudingerweg 9, D-55099 Mainz, Germany, Laboratoire L. Neel-CNRS, BP 166, 25 Avenue des Martyrs, 38042 Grenoble Cedex 9, France, Laboratoire de Cristallographie, Institut de Chimie, Université de Neuchâtel, Avenue de Bellevaux 51, C.P. 2, Neuchâtel CH-2007, Switzerland, and Laboratory for Neutron Scattering, PSI and ETHZ, Villigen PSI CH-5232, Switzerland

Received March 25, 2004

Nine members of a new family of polynuclear ferric complexes have been synthesized and characterized. The reaction of $Fe(O_2CMe)_2$ with polydentate Schiff base proligands (H_2L) derived from salicylidene-2-ethanolamine, followed in some cases by reaction with carboxylic acids, has afforded new complexes of general formulas $[Fe_2(pic)_2(L)_2]$ (where pic^- is the anion of 2-picolinic acid), $[Fe_3(O_2CMe)_3(L)_3]$, $[Fe_4(OR)_2(O_2CMe)_2(L)_4]$, and $[Fe_5O(OH)(O_2CR)_4(L)_4]$. The tri-, tetra-, and pentanuclear complexes all possess unusual structures and novel core topologies. Mössbauer spectroscopy confirms the presence of high-spin ferric centers in the tri- and pentanuclear complexes. Variable-temperature magnetic measurements suggest spin ground states of $S = 0$, 1/2, 0, and 5/2 for the bi-, tri-, tetra-, and pentanuclear complexes, respectively. Fits of the magnetic susceptibility data have provided the magnitude of the exclusively antiferromagnetic exchange interactions. In addition, an easy-axis-type magnetic anisotropy has been observed for the pentanuclear complexes, with D values of approximately -0.4 cm^{-1} determined from modeling the low-temperature magnetization data. A low-temperature micro-SQUID study of one of the pentanuclear complexes reveals magnetization hysteresis at nonzero field. This is attributed to an anisotropy-induced energy barrier to magnetization reversal that is of molecular origin. Finally, an inelastic neutron scattering study of one of the trinuclear complexes has revealed that the magnetic behavior arises from two distinct species.

Introduction

The considerable current interest in polynuclear ferric complexes arises from their relevance to diverse fields ranging from bioinorganic chemistry to molecular magnetic materials. In biological systems oxo-, hydroxo-, and carboxylato-bridged Fe centers play an important role in the active sites of various non-heme Fe proteins.[1] Proteins such as hemerythrin (Hr), methane monoxygenase (MMO), and ribonucleotide reductase contain similar (μ-oxo or μ-hydroxo)(μ-carboxylato)diiron cores, despite the disparate functions that they perform (e.g., oxygen transport for Hr and catalytic oxidation for MMO). On a larger scale, the iron storage protein ferritin has a ferric oxyhydroxide core containing up to 4500 Fe centers. This core is formed inside the preassembled protein shell upon oxidation and hydrolysis of Fe^{II}. Amino acids featuring carboxylate residues are believed to play a key role in this process. As a result, a number of polynuclear $\{Fe_x\}$ ($x = 11$, 12, 17, 19) complexes featuring oxo, hydroxo, and carboxylato ligation have been synthesized and studied as possible models for ferritin to gain a better understanding of the biomineralization process involved in the formation of its metal core.[2,3]

Oxo- and hydroxo-bridged diiron units typically display antiferromagnetic exchange interactions.[4] For polynuclear Fe

* Author to whom correspondence should be addressed. Present address: School of Chemistry, University of Melbourne, Parkville, Victoria 3010, Australia. E-mail: c.boskovic@unimelb.edu.au.
† Universität Bern.
‡ Johannes Gutenberg Universität.
§ Laboratoire L. Neel-CNRS.
|| Université de Neuchâtel.
⊥ PSI and ETHZ.

(1) Crichton, R. R. *Inorganic Biochemistry of Iron Metabolism*; Horwood: New York, 1991.

10.1021/ic049600f CCC: $27.50
Published on Web 07/10/2004

complexes ($\{Fe_x\}$, $x > 2$), uncompensated spins or spin frustration associated with competing antiferromagnetic interactions can lead to molecules with a nonzero magnetic moment and interesting magnetic behavior. Low-temperature Mössbauer spectroscopy in zero field of some of the complexes proposed as models of ferritin reveals magnetic splitting associated with slow relaxation of the magnetization (reorientation of the magnetization direction).[2,5] This has been attributed to superparamagnetic behavior akin to that observed for the ferritin core itself.[6] Such superparamagnetism occurs for small particles of ordered materials (<100 Å). These are of the dimension of a single magnetic domain, where the small particle size renders the magnetic moment unstable to thermal fluctuations. For such particles, the energy barrier to magnetization relaxation depends on the volume and shape of the particle. However, the thermal scrambling of the magnetic dipole is offset, and slow magnetic relaxation is observed below a characteristic "blocking temperature", which is dependent on the time scale of the measurement technique.

Interestingly, similar slow magnetization relaxation has been observed in the low-temperature zero-field Mössbauer spectra of the ferric compounds $[Fe_4(OMe)_6(dpm)_6]$ and $[Fe_8O_2(OH)_{12}(tacn)_6]Br_8$.[7] However, for these species, the slow relaxation has been attributed to a completely different process. Both of these complexes possess a relatively high spin ground state ($S = 5$ and 10 for the tetra- and octanuclear complexes, respectively) in addition to a significant magnetic anisotropy. This results in an anisotropy-induced energy barrier to thermal relaxation of the magnetization that is of purely molecular origin.[8−10] These compounds have been described as "single-molecule magnets" (SMMs).[11] In general, for SMMs with a large-spin ground state (S) and a large easy-axis-type magnetic anisotropy ($D < 0$, where D is the axial zero-field splitting parameter), the energy barrier to magnetization relaxation is given to first order by $S^2|D|$ or $(S^2 - 1/4)|D|$, for integer and half-integer spins, respectively. Other $\{Fe^{III}_x\}$ ($x = 11$, 17, 19) complexes have also been identified as SMMs.[12,13] For such materials the magnetic bistability arising from this energy barrier suggests tremendous potential for applications in information storage devices, whereby a single molecule could act as the smallest possible unit of magnetic memory. Furthermore, quantum tunneling of the magnetization through the energy barrier has been observed for a number of SMMs, and it has been proposed that this may ultimately provide the superposition of logic states necessary for SMMs to act as qubits in quantum computers.[14]

With this in mind we have turned our attention to the application of the Schiff base proligand salicylidene-2-ethanolamine (H_2L^1) and its derivatives H_2L^2 and H_2L^3 (Chart 1) to the chemistry of iron.

Chart 1

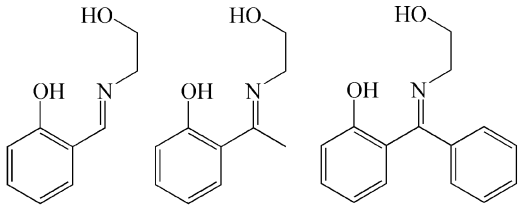

H_2L^1 H_2L^2 H_2L^3

Preliminary results of this study have been communicated previously.[15,16] Deprotonation of the proligands affords the potentially tridentate mono- and bianionic ligands. Each incorporates an ONO donor set and possesses the ability to bind in both bridging and chelating modes, enhancing the stability of the metal complexes formed. The ligands favor binding in a meridional fashion, as has been observed in a number of mono- and binuclear transition-metal species.[17] In addition, we have recently reported that a family of tetranuclear Mn complexes bearing $(L^1)^{2-}$ and its derivatives function as SMMs,[18] while a tetranuclear Fe^{II} complex of $(L^1)^{2-}$ has also been reported to display SMM behavior.[19] Finally, we have communicated the synthesis and preliminary magnetic characterization of a tetranuclear Ni^{II} complex of $(L^1)^{2-}$,[15] while tetranuclear Cu and Mn complexes and hexanuclear Mn complexes of the same ligand have been reported previously.[20]

(2) (a) Gorun, S. M.; Papaefthymiou, G. C.; Frankel, R. B.; Lippard, S. J. *J. Am. Chem. Soc.* **1987**, *109*, 3337. (b) Taft, K. L.; Papaefthymiou, G. C.; Lippard, S. J. *Science* **1993**, *259*, 1302. (c) Taft, K. L.; Papaefthymiou, G. C.; Lippard, S. J. *Inorg. Chem.* **1994**, *33*, 1510. (d) Caneschi, A.; Cornia, A.; Lippard, S. J.; Papaefthymiou, G. C.; Sessoli, R. *Inorg. Chim. Acta* **1996**, *243*, 295.

(3) Powell, A. K.; Heath, S. L.; Gatteschi, D.; Pardi, L.; Sessoli, R.; Spina, G.; Del Giallo, F.; Pieralli, F. *J. Am. Chem. Soc.* **1995**, *117*, 2491.

(4) Kurtz, D. M. *Chem. Rev.* **1990**, *90*, 585.

(5) Papaefthymiou, G. C. *Phys. Rev. B* **1992**, *46*, 366.

(6) St. Pierre, T. G.; Dickson, D. P. E.; Webb, J.; Kim, K. S.; Macey, D. J.; Mann, S. *Hyperfine Interact.* **1986**, *29*, 1427.

(7) (a) Barra, A.-L.; Debrunner, P.; Gatteschi, D.; Schulz, C. E.; Sessoli, R. *Europhys. Lett.* **1996**, *35*, 133. (b) Caneschi, A.; Cianchi, L.; Del Giallo, F.; Gatteschi, D.; Moretti, P.; Pieralli, F.; Spina, G. *J. Phys.: Condens. Matter* **1999**, *11*, 3395. (c) Cianchi, L.; Del Giallo, F.; Spina, G.; Reiff, W.; Caneschi, A. *Phys. Rev. B* **2002**, *65*, 064415.

(8) Barra, A. L.; Caneschi, A.; Cornia, A.; De Biani, F. F.; Gatteschi, D.; Sangregorio, C.; Sessoli, R.; Sorace, L. *J. Am. Chem. Soc.* **1999**, *121*, 5302.

(9) Sangregorio, C.; Ohm, T.; Paulsen, C.; Sessoli, R.; Gatteschi, D. *Phys. Rev. Lett.* **1997**, *78*, 4645.

(10) Gatteschi, D.; Sessoli, R.; Cornia, A. *Chem. Commun.* **2000**, 725.

(11) Gatteschi, D.; Sessoli, R. *Angew. Chem., Int. Ed.* **2003**, *42*, 268 and references therein.

(12) Jones, L. F.; Brechin, E. K.; Collison, D.; Helliwell, M.; Mallah, T.; Piligkos, S.; Rajaraman, G.; Wernsdorfer, W. *Inorg. Chem.* **2003**, *42*, 6601.

(13) Goodwin, J. C.; Sessoli, R.; Gatteschi, D.; Wernsdorfer, W.; Powell, A. K.; Heath, S. L. *J. Chem. Soc., Dalton Trans.* **2000**, 1835.

(14) Leuenberger, M. N.; Loss, D. *Nature* **2000**, *410*, 789.

(15) (a) Boskovic, C.; Rusanov, E.; Stoeckli-Evans, H.; Güdel, H. U. *Inorg. Chem. Commun.* **2002**, *5*, 881. (b) Basler, R.; Boskovic, C.; Chaboussant, G.; Güdel, H. U.; Murrie, M.; Ochsenbein, S. T.; Sieber, A. *ChemPhysChem* **2003**, *4*, 910.

(16) Boskovic, C.; Labat, G.; Neels, A.; Güdel, H. U. *Dalton Trans.* **2003**, 3671.

(17) (a) Asada, H.; Ozeki, M.; Fujiwara, M.; Matsushita, T. *Chem. Lett.* **1999**, 525. (b) Dey, M.; Rao, C. P.; Saarenketo, P. K.; Rissanen, K. *Inorg. Chem. Commun.* **2002**, *5*, 924.

(18) Boskovic, C.; Bircher, R.; Tregenna-Piggott, P. L. W.; Güdel, H. U.; Paulsen, C.; Wernsdorfer, W.; Barra, A. L.; Khatsko, E.; Neels, A.; Stoeckli-Evans, H. *J. Am. Chem. Soc.* **2003**, *125*, 14046.

(19) Oshio, H.; Hoshino, N.; Ito, T. *J. Am. Chem. Soc.* **2000**, *120*, 2997.

(20) (a) Chumakov, Y. M.; Biyushkin, V. N.; Malinovskii, T. I.; Kulemu, S.; Tsapkov, V. I.; Popov, M. S.; Samus, N. M. *Koord. Khim.* **1990**, *16*, 945. (b) Hoshino, N.; Ito, T.; Nihei, M.; Oshio, H. *Inorg. Chem. Commun.* **2003**, *6*, 377.

Experimental Section

Syntheses. All manipulations were performed under aerobic conditions, using materials as received. H_2L^1 was prepared as described;[15a] H_2L^2 and H_2L^3 were synthesized in an analogous manner. picH is 2-picolinic acid.

$[Fe_2(pic)_2(L^1)_2]$ (1). picH (0.15 g, 1.2 mmol) was added to a solution of compound **2** (0.50 g, 0.60 mmol) in MeCN, and the resulting mixture was stirred for several hours, affording a red precipitate. This was recrystallized by layering a concentrated CH_2Cl_2 solution with hexane to give dark red blocklike crystals. These were isolated by filtration and washed with hexane; yield 90%. A sample for crystallography was maintained in contact with the mother liquor to prevent the loss of interstitial solvent. Drying under vacuum at room temperature afforded a partially solvated sample. Anal. Calcd for $[Fe_2(pic)_2(L^1)_2]\cdot CH_2Cl_2$, $C_{31}H_{28}N_4Fe_2O_8Cl_2$: C, 48.53; H, 3.68; N, 7.30. Found: C, 48.70; H, 3.72; N, 7.11. The solvation levels were confirmed by thermogravimetric analysis. Selected IR data (cm^{-1}): 1668 (s), 1654 (m), 1629 (s), 1600 (s), 1571 (w), 1546 (m), 1471 (m), 1448 (m), 1410 (m), 1347 (s), 1339 (s), 1305 (m), 1289 (s), 1257 (w), 1234 (w), 1199 (m), 1168 (m), 1148 (m), 1123 (w), 1093 (w), 1063 (w), 1046 (s), 1033 (m), 1023 (m), 936 (w), 899 (m), 850 (m), 796 (w), 761 (m), 707 (m), 694 (m), 647 (w), 618 (m), 519 (m), 481 (w), 467 (w), 440 (w), 420 (m).

$[Fe_3(O_2CMe)_3(L^1)_3]$ (2). $Fe(OAc)_2$ (0.43 g, 2.5 mmol) was added to a solution of H_2L^1 (0.41 g, 2.5 mmol) in EtOH (40 cm^3), and the resulting mixture was stirred overnight, affording a red-brown precipitate. This was recrystallized by layering a concentrated CH_2Cl_2 solution with hexane, to give dark red rodlike crystals. These were isolated by filtration and washed with hexane; yield 75%. A sample for crystallography was maintained in contact with the mother liquor to prevent the loss of interstitial solvent. Drying under vacuum at room temperature afforded a partially solvated sample. Anal. Calcd for $[Fe_3(O_2CMe)_3(L^1)_3]\cdot 0.5CH_2Cl_2$, $C_{33.5}H_{37}N_3Fe_3O_{12}Cl_1$: C, 45.90; H, 4.25; N, 4.79. Found: C, 46.11; H, 4.25; N, 4.41. Drying under vacuum at 80 °C afforded a fully desolvated sample. Anal. Calcd for $[Fe_3(O_2CMe)_3(L^1)_3]$, $C_{33}H_{36}N_3Fe_3O_{12}$: C, 47.51; H, 4.35; N, 5.04. Found: C, 47.52; H, 4.40; N, 5.07. The solvation levels were confirmed by thermogravimetric analysis. Selected IR data (cm^{-1}): 1639 (s), 1601 (m), 1560 (s), 1469 (m), 1449 (s), 1430 (s, sh), 1389 (m), 1337 (m), 1310 (m), 1219 (w), 1198 (w), 1148 (m), 1126 (w), 1066 (w), 1043 (m), 1030 (m), 931 (w), 901 (w), 878 (w), 857 (w), 794 (w), 759 (m), 739 (w), 660 (m), 643 (w), 613 (m), 560 (m), 545 (m), 412 (m).

$[Fe_3(O_2CMe)_3(L^2)_3]$ (3). $Fe(OAc)_2$ (0.43 g, 2.5 mmol) was added to a solution of H_2L^2 (0.45 g, 2.5 mmol) in EtOH (40 cm^3), and the resulting mixture was stirred overnight, affording a red-brown precipitate. This crude product was isolated by filtration and washed with EtOH; yield 85%. Drying under vacuum at room temperature afforded a partially hydrated sample. Anal. Calcd for $[Fe_3(O_2CMe)_3(L^2)_3]\cdot 2H_2O$, $C_{36}H_{46}N_3Fe_3O_{14}$: C, 47.40; H, 5.08; N, 4.61. Found: C, 47.22; H, 5.16; N, 4.12. The solvation level was confirmed by thermogravimetric analysis. Selected IR data (cm^{-1}): 1601 (s), 1560 (s), 1543 (s), 1473 (w), 1440 (s), 1370 (w), 1327 (m), 1260 (w), 1237 (m), 1161 (w), 1136 (w), 1080 (w), 1067 (m), 1057 (m), 1021 (w), 984 (w), 928 (w), 879 (w), 848 (w), 752 (m), 659 (m), 615 (w), 604 (m), 592 (m), 561 (m), 524 (w), 490 (w), 419 (m).

$[Fe_3(O_2CMe)_3(L^3)_3]$ (4). $Fe(OAc)_2$ (0.43 g, 2.5 mmol) was added to a solution of H_2L^3 (0.60 g, 2.5 mmol) in MeCN (60 cm^3), and the resulting mixture was stirred overnight, affording a red-brown precipitate. This was recrystallized by layering a concentrated CH_2Cl_2 solution with hexane to give dark red crystals. These were isolated by filtration and washed with hexane; yield 70%. A sample for crystallography was maintained in contact with the mother liquor to prevent the loss of interstitial solvent. Drying under vacuum at 100 °C afforded a fully desolvated sample. Anal. Calcd for $[Fe_3(O_2CMe)_3(L^3)_3]$, $C_{51}H_{48}N_3Fe_3O_{12}$: C, 57.65; H, 4.55; N, 3.95. Found: C, 57.61; H, 4.64; N, 3.73. The solvation level was confirmed by thermogravimetric analysis. Selected IR data (cm^{-1}): 1599 (m), 1565 (s), 1539 (s), 1491 (w), 1463 (m), 1439 (s), 1420 (m, sh), 1366 (w), 1359 (w), 1331 (s), 1261 (m), 1247 (m), 1144 (m), 1121 (w), 1061 (m), 1052 (m), 1042 (m), 1024 (w), 963 (w), 908 (m), 849 (m), 777 (w), 758 (m), 749 (m), 736 (w), 705 (m), 653 (w), 638 (w), 614 (m), 595 (m), 524 (w), 509 (w), 457 (w), 441 (w).

$[Fe_4(OMe)_2(O_2CMe)_2(L^3)_4]$ (5). Method 1. A concentrated solution of crude **4** in MeOH was layered with Et_2O to produce red-brown crystals together with an amorphous pale-colored byproduct. These were isolated by filtration and washed with EtOH; however, removal of the byproduct proved impossible. A sample for crystallography was maintained in contact with the mother liquor to prevent the loss of interstitial solvent. Selected IR data (cm^{-1}): 1598 (s), 1586 (s), 1564 (s), 1534 (s), 1491 (w), 1464 (m), 1441 (s), 1415 (m, sh) 1363 (w), 1340 (s), 1328 (m), 1260 (m), 1248 (m), 1238 (m), 1145 (m), 1120 (w), 1091 (w), 1059 (m), 1040 (m), 1026 (m), 961 (w), 905 (m), 848 (m), 775 (w), 747 (m), 725 (w), 701 (m), 693 (m), 653 (w), 636 (w), 611 (m), 587 (m), 556 (m), 533 (w), 508 (m), 492 (m), 453 (m).

Method 2. $Fe(OAc)_2$ (0.43 g, 2.5 mmol) was added to a solution of H_2L^3 (0.60 g, 2.5 mmol) in MeOH (40 cm^3), and the resulting mixture was stirred overnight, affording a red-brown precipitate. This crude product was isolated by filtration and washed with MeOH; yield 90%. IR spectroscopy indicated that this material was identical with that obtained by method 1.

$[Fe_4(OEt)_2(O_2CMe)_2(L^3)_4]$ (6). Method 1. A concentrated solution of crude **4** in EtOH was allowed to stand in a sealed vessel to produce red-brown crystals. These were isolated by filtration and washed with EtOH; yield 25%. The sample was dried overnight under vacuum at 110 °C, but appears to be hygroscopic. Anal. Calcd for $[Fe_4(OEt)_2(O_2CMe)_2(L^3)_4]\cdot H_2O$, $C_{68}H_{70}N_4Fe_4O_{15}$: C, 58.06; H, 5.02; N, 3.98. Found: C, 57.94; H, 4.82; N, 3.77. The solvation level was confirmed by thermogravimetric analysis. Selected IR data (cm^{-1}): 1597 (s), 1586 (sh), 1568 (s), 1536 (s), 1491 (w), 1463 (m), 1441 (s), 1415 (m, sh) 1363 (w), 1340 (s), 1328 (m), 1260 (m), 1247 (m), 1146 (m), 1121 (w), 1082 (w), 1054 (m), 1040 (m), 1027 (m), 963 (w), 905 (m), 849 (m), 776 (w), 749 (m), 726 (w), 702 (m), 654 (w), 636 (w), 612 (m), 587 (m), 559 (m), 533 (w), 508 (w), 497 (m), 445 (m).

Method 2. $Fe(OAc)_2$ (0.43 g, 2.5 mmol) was added to a solution of H_2L^3 (0.60 g, 2.5 mmol) in EtOH (40 cm^3), and the resulting mixture was stirred overnight, affording a red-brown precipitate. This crude product was isolated by filtration and washed with EtOH; yield 90%. IR spectroscopy indicated that this material was identical with that obtained by method 1.

$[Fe_5O(OH)(O_2CC_6H_4\text{-}p\text{-}NO_2)_4(L^1)_4]$ (7). A slurry of **2** (0.50 g, 0.60 mmol) in MeCN/toluene (1:1, 50 cm^3) was treated with p-$NO_2C_6H_4CO_2H$ (0.30 g, 1.8 mmol) and evaporated to dryness. The resulting residue was redissolved in toluene and evaporated to dryness two more times before being recrystallized by layering a concentrated solution in toluene with hexane, to give dark brown crystals. These were isolated by filtration and washed with toluene; yield 25%. A sample for crystallography was maintained in contact with the mother liquor to prevent the loss of interstitial solvent. Drying under vacuum at 45 °C afforded a fully desolvated sample. Anal. Calcd for $[Fe_5O(OH)(O_2CC_6H_4\text{-}p\text{-}NO_2)_4(L^1)_4]$, $C_{64}H_{53}N_8Fe_5O_{26}$: C, 47.18; H, 3.28; N, 6.88. Found: C, 47.13; H, 3.28; N,

Table 1. Crystallographic Data for **1**·CH_2Cl_2, **2**·CH_2Cl_2, **4**·CH_2Cl_2, and **5**·0.5MeOH

	1·CH_2Cl_2	**2**·CH_2Cl_2	**4**·CH_2Cl_2	**5**·0.5MeOH
empirical formula	$C_{31}H_{28}Cl_2Fe_2N_4O_8$	$C_{34}H_{38}Cl_2Fe_3N_3O_{12}$	$C_{52}H_{50}Cl_2Fe_3N_3O_{12}$	$C_{66.5}H_{66}Fe_4N_4O_{145}$
fw	767.17	919.12	1147.40	1376.63
space group	*C*2/*c*	*Pca*2$_1$	*P*2$_1$/*c*	*P*2/*c*
a, Å	13.4247(12)	17.9897(8)	9.7371(11)	17.3156(14)
b, Å	16.7179(16)	13.8773(6)	40.685(4)	8.0980(6)
c, Å	14.9140(11)	31.0893(19)	13.1279(15)	25.702(3)
α, deg	90	90	90	90
β, deg	100.225(10)	90	106.802(9)	118.058(7)
γ, deg	90	90	90	90
V, Å^3	3294.0(5)	7761.4(7)	4978.6(9)	3180.4(5)
Z	4	8	4	2
T, K	153(2)	153(2)	153(2)	153(2)
λ, Å	0.71073	0.71073	0.71073	0.71073
ρ_{calcd}, g cm^{-3}	1.547	1.573	1.531	1.438
μ, mm^{-1}	1.099	1.308	1.037	0.963
no. of obsd data [$I > 2\sigma(I)$]	2006	9064	3659	3850
R1[a]	0.0316	0.0455	0.1026	0.0398
wR2	0.0571[b]	0.1065[c]	0.2083[d]	0.0928[e]

[a] $R1 = \sum||F_o| - |F_c||/\sum|F_o|$. [b] $wR2 = [\sum w(F_o^2 - F_c^2)^2/\sum wF_o^4]^{1/2}$; $w = 1/[\sigma^2(F_o^2) + (0.0257P)^2]$, where $P = (F_o^2 + 2F_c^2)/3$. [c] $wR2 = [\sum w(F_o^2 - F_c^2)^2/\sum wF_o^4]^{1/2}$; $w = 1/[\sigma^2(F_o^2) + (0.1P)^2]$, where $P = (F_o^2 + 2F_c^2)/3$. [d] $wR2 = [\sum w(F_o^2 - F_c^2)^2/\sum wF_o^4]^{1/2}$; $w = 1/[\sigma^2(F_o^2) + (0.0974P)^2]$, where $P = (F_o^2 + 2F_c^2)/3$. [e] $wR2 = [\sum w(F_o^2 - F_c^2)^2/\sum wF_o^4]^{1/2}$; $w = 1/[\sigma^2(F_o^2) + (0.0552P)^2]$, where $P = (F_o^2 + 2F_c^2)/3$.

6.65. The lack of solvation was confirmed by thermogravimetric analysis. Selected IR data (cm^{-1}): 1642 (s), 1616 (m), 1601 (m), 1563 (s), 1545 (s), 1524 (m), 1470 (m), 1450 (s), 1345 (s), 1317 (m), 1270 (w), 1230 (w), 1219 (w), 1200 (w), 1150 (m), 1128 (w), 1104 (w), 1076 (w), 1045 (m), 1015 8w), 978 (w), 931 (w), 902 (w), 877 (w), 863 (w), 828 (m), 795 (m), 759 (m), 725 (m), 642(w), 623 (m), 613 (m), 558 (m), 533 (m).

[$Fe_5O(OH)(O_2CMe)_4(L^2)_4$] (8). A concentrated solution of crude **3** in CH_2Cl_2 was layered with hexane to afford dark brown crystals. These were isolated by filtration and washed with hexane; yield 80%. A sample for crystallography was maintained in contact with the mother liquor to prevent the loss of interstitial solvent. Drying under vacuum at room temperature and exposure to air afforded a hydrated sample. Anal. Calcd for $[Fe_5O(OH)(O_2CMe)_4(L^2)_4]\cdot H_2O$, $C_{48}H_{59}N_4Fe_5O_{19}$: C, 45.21; H, 4.66; N, 4.39. Found: C, 45.16; H, 4.86; N, 4.34. The hydration level was confirmed by thermogravimetric analysis. Selected IR data (cm^{-1}): 1600 (s), 1560 (s), 1542 (s), 1473 (m), 1442 (s), 1420 (s), 1367 (m), 1324 (s), 1293 (m), 1259 (w), 1235 (m), 1163 (w), 1138 (w), 1100 (w), 1069 (m), 1019 (m), 983 (w), 922 (w), 880 (w), 846 (m), 757 (m), 670 (m), 656 (m), 601 (m), 563 (m), 523 (m), 494 (m), 421 (w).

[$Fe_5O(OH)(O_2CPh)_4(L^3)_4$] (9). A solution of **4** (0.25 g, 0.24 mmol) in CH_2Cl_2/toluene (1:1, 50 cm^3) was treated with $PhCO_2H$ (0.18 g, 1.5 mmol) and evaporated to dryness. The resulting residue was redissolved in toluene and evaporated to dryness two more times before being recrystallized by layering a concentrated solution in toluene with hexane, to give dark brown crystals. These were isolated by filtration and washed with toluene; yield 40%. A sample for crystallography was maintained in contact with the mother liquor to prevent the loss of interstitial solvent. Drying under vacuum at room temperature followed by exposure to air afforded a hydrated sample. Anal. Calcd for $[Fe_5O(OH)(O_2CPh)_4(L^3)_4]\cdot 2H_2O$, $C_{88}H_{77}N_4Fe_5O_{20}$: C, 59.05; H, 4.34; N, 3.13. Found: C, 59.11; H, 4.31; N, 2.79. The hydration level was confirmed by thermogravimetric analysis. Selected IR data (cm^{-1}): 1619 (m), 1593 (s), 1540 (s), 1523 (s), 1492 (m), 1464 (m), 1441 (s), 1397 (s), 1326 (s), 1293 (w), 1242 (m), 1175 (w), 1146 (m), 1121 (w), 1093 (w), 1070 (m), 1052 (m), 1042 (m), 1026 (m), 956 (w), 903 (w) 848 (m), 777 (w), 753 (m), 725 (m), 718 (m), 702 (m), 690 (m), 676 (m), 639 (w), 621 (m), 598 (m), 556 (w), 539 (w), 504 (w), 464 (m), 438 (m).

X-ray Crystallography. The intensity data of compounds **1**·CH_2Cl_2, **2**·CH_2Cl_2, **4**·CH_2Cl_2, **5**·0.5MeOH, **7**·H_2O·C_7H_8·0.5C_6H_{14}, **8**·0.25H_2O·4.5CH_2Cl_2, and **9**·1.5H_2O·2CH_2Cl_2·0.5C_2H_4O were collected at 153 K on Stoe image plate diffraction systems I and II[21] using Mo Kα graphite-monochromated radiation. Compound **1**·CH_2Cl_2 employed image plate I, distance 70 mm, ϕ oscillation scans 0−199.5°, step $\Delta\phi = 1.5°$, $d_{min} - d_{max} = 12.45 - 0.81$ Å. Compound **2**·CH_2Cl_2 employed image plate I, distance 70 mm, ϕ oscillation scans 0−100°, step $\Delta\phi = 0.8°$, $d_{min} - d_{max} = 12.45 - 0.81$ Å. Compound **4**·CH_2Cl_2 employed image plate II, distance 140 mm, 120 frames with $\phi = 0°$ and $0° < \omega < 180°$ and 120 frames with $\phi = 90°$ and $0° < \omega < 180°$, with the crystal oscillating through 1.5° in ω. The resolution was $d_{min} - d_{max} = 17.78 - 0.72$ Å. Compound **5**·0.5MeOH employed image plate I, distance 70 mm, ϕ oscillation scans 0−180°, step $\Delta\phi = 1°$, $d_{min} - d_{max} = 12.45 - 0.81$ Å. Compound **7**·H_2O·C_7H_8·0.5C_6H_{14} employed image plate II, distance 140 mm, 180 frames with $\phi = 0°$ and $0° < \omega < 180°$ and 44 frames with $\phi = 90°$ and $0° < \omega < 44°$, with the crystal oscillating through 1° in ω. The resolution was $d_{min} - d_{max} = 24.88 - 0.83$ Å. Compound **8**·0.25H_2O·4.5CH_2Cl_2 and compound **9**·1.5H_2O·2CH_2Cl_2·0.5C_2H_4O employed image plate I, distance 70 mm, ϕ oscillation scans 0−180°, step $\Delta\phi = 1°$, $d_{min} - d_{max} = 12.45 - 0.81$ Å. The structures of all compounds were solved by direct methods using the program SHELXS-97[22] and refined using weighted full-matrix least-squares on F^2. The refinement and all further calculations were carried out using SHELXL-97.[23] Crystallographic data for **1**·CH_2Cl_2, **2**·CH_2Cl_2, **4**·CH_2Cl_2, **5**·0.5MeOH, **7**·H_2O·C_7H_8·0.5C_6H_{14}, **8**·0.25H_2O·4.5CH_2Cl_2, and **9**·1.5H_2O·2CH_2Cl_2·0.5C_2H_4O are given in Tables 1 and 2.

For compound **1**·CH_2Cl_2 the H atoms were located from Fourier difference maps and refined isotropically. For compounds **2**·CH_2Cl_2, **4**·CH_2Cl_2, and **5**·0.5MeOH the H atoms were included in calculated positions and treated as riding atoms using SHELXL default parameters. For compound **7**·H_2O·C_7H_8·0.5C_6H_{14} the position of the hydroxo H atom was located from Fourier difference maps and freely refined, while the remaining H atoms were included in calculated positions and treated as riding atoms using SHELXL default parameters. For compounds **8**·0.25H_2O·4.5CH_2Cl_2 and **9**·

(21) Stoe & Cie. *IPDS Software*; Stoe & Cie GmbH: Darmstadt, Germany, 2000.
(22) Sheldrick, G. M. SHELXS-97 Program for Crystal Structure Determination. *Acta Crystallogr.* **1990**, *A46*, 467.
(23) Sheldrick, G. M. *SHELXL-97, Program for Crystal Structure Refinement*; Universität Göttingen: Göttingen, Germany, 1999.

Table 2. Crystallographic Data for **7**·H_2O·C_7H_8·0.5C_6H_{14}, **8**·0.25H_2O·4.5CH_2Cl_2, and **9**·1.5H_2O·2CH_2Cl_2·0.5C_2H_4O

	7·H_2O·C_7H_8·0.5C_6H_{14}	**8**·0.25H_2O·4.5CH_2Cl_2	**9**·1.5H_2O·2CH_2Cl_2·0.5C_2H_4O
empirical formula	$C_{74}H_{70}Fe_5N_8O_{27}$	$C_{52.5}H_{66.5}Cl_9Fe_5N_4O_{18.25}$	$C_{90.5}H_{82}Cl_4Fe_5N_4O_{20}$
fw	1782.63	1643.90	1966.65
space group	$P\bar{1}$	$P\bar{1}$	$P\bar{1}$
a, Å	15.3288(9)	14.6913(12)	14.4742(13)
b, Å	15.9751(10)	23.5238(18)	15.4790(15)
c, Å	20.0357(13)	23.4482(18)	21.1155(18)
α, deg	104.081(5)	62.310(8)	87.069(11)
β, deg	99.318(5)	88.319(10)	79.397(10)
γ, deg	116.649(4)	72.627(9	69.702(10)
V, Å^3	4040.1(4)	6790.5(9)	4360.9(7)
Z	2	4	2
T, K	153(2)	153(2)	153(2)
λ, Å	0.71073	0.71073	0.71073
ρ_{calcd}, g cm^{-3}	1.465	1.608	1.498
μ, mm^{-1}	0.959	1.465	1.008
no. of obsd data [$I > 2\sigma(I)$]	9976	13533	10027
R1[a]	0.0588	0.0834	0.0584
wR2	0.1597[b]	0.2130[c]	0.1676[d]

[a] $R1 = \sum||F_o| - |F_c||/\sum|F_o|$. [b] $wR2 = [\sum w(F_o^2 - F_c^2)^2/\sum wF_o^4]^{1/2}$; $w = 1/[\sigma^2(F_o^2) + (0.1174P)^2]$, where $P = (F_o^2 + 2F_c^2)/3$. [c] $wR2 = [\sum w(F_o^2 - F_c^2)^2/\sum wF_o^4]^{1/2}$; $w = 1/[\sigma^2(F_o^2) + (0.1372P)^2]$, where $P = (F_o^2 + 2F_c^2)/3$. [d] $wR2 = [\sum w(F_o^2 - F_c^2)^2/\sum wF_o^4]^{1/2}$; $w = 1/[\sigma^2(F_o^2) + (0.1021P)^2]$, where $P = (F_o^2 + 2F_c^2)/3$.

1.5H_2O·2CH_2Cl_2·0.5C_2H_4O the positions of the hydroxo H atoms were derived from Fourier difference maps and refined with the O−H distance constrained to the theoretical value, while the remaining H atoms were included in calculated positions and treated as riding atoms using SHELXL default parameters. The non-H atoms were refined anisotropically for all compounds except for one MeOH molecule (25% occupied) of **5**·0.5MeOH, C104 (50% occupied) of **8**·0.25H_2O·4.5CH_2Cl_2, and partially occupied MeOH and H_2O atoms of **9**·1.5H_2O·2CH_2Cl_2·0.5C_2H_4O, which were refined isotropically.

For compound **2**·CH_2Cl_2 the structure was refined as a racemic twin with a final refined BASF (batch scale factor) value of 0.40(2). A multiscan absorption correction was applied for compounds **4**·CH_2Cl_2 and **5**·0.5MeOH using the MULABS routine in PLATON,[24] and an empirical absorption correction was applied for compounds **8**·0.25H_2O·4.5CH_2Cl_2 and **9**·1.5H_2O·2CH_2Cl_2·0.5C_2H_4O using the DIFABS routine in PLATON.

Magnetic Measurements. Variable-temperature magnetic susceptibility measurements down to 1.8 K were performed with a Quantum Design MPMS-XL susceptometer equipped with a 5 T magnet. Data were collected on powdered crystals. Pascal's constants were used to estimate the diamagnetic correction for each complex. Low-temperature magnetic measurements were performed on single crystals using an array of micro-SQUIDS.[25] Measurements were performed on this magnetometer in the temperature range 0.04−7.0 K, with fields up to 1.4 T. The field can be applied in any direction by separately driving three orthogonal coils. The experimental susceptibility data were fit using the Levenberg−Marquardt least-squares fitting algorithm, in combination with MAGPACK, which employs matrix diagonalization methods and the isotropic Heisenberg−Dirac−Van Vleck term as the leading part of the exchange spin Hamiltonian.[26] χ_M vs *T* and $\chi_M T$ vs *T* data were fit separately and the results combined to give the final fitting parameters.

Inelastic Neutron Scattering (INS) Studies. INS spectra were recorded on the time-of-flight spectrometer FOCUS at the SINQ facility (PSI, Switzerland) with wavelengths of $\lambda_i = 3.8$ Å and $\lambda_i = 4.3$ Å. Approximately 3 g of an undeuterated, polycrystalline sample was sealed under helium in an aluminum container of size 40 × 40 × 3 mm^3. The data treatment involved a calibration of the detectors using a spectrum of vanadium metal and a background subtraction using an empty can. The time-of-flight to energy conversion and the data reduction were performed using the standard program Nathan. Further data treatment employed the program Igor-Pro 4.0.2.1 (Wave Metrics).

Mössbauer Spectroscopy. A constant-acceleration-type Mössbauer spectrometer equipped with a 1024-channel analyzer operating in the time scale mode, and a 25 mCi ^{57}Co/Rh source, was employed. The isomer shifts reported here are relative to that of α-Fe at room temperature. Spectra of the sample (thickness of about 5 mg of Fe/cm^2) were collected between 293 and 4.2 K by means of a combined He continuous flow/bath cryostat. The Mössbauer spectra were analyzed using the computer program EFFINO.[27]

Other Measurements. Infrared spectra (KBr disk) were recorded on a Perkin-Elmer Spectrum One FTIR spectrometer. Elemental analyses were performed at the Ecole d'ingénieurs et d'architectes de Fribourg, Switzerland.

Results

Syntheses. The transformations involving complexes **1**−**9** are summarized in Scheme 1.

Overnight treatment of a slurry of $Fe(OAc)_2$ in EtOH with 1 equiv of H_2L^1 or H_2L^2 affords the trinuclear complexes **2** and **3**, respectively, while a similar reaction with H_2L^3 in MeCN affords trinuclear **4**. In each case the yields are high. The reaction may be written as

$$3Fe(O_2CMe)_2 + 3H_2L \rightarrow [Fe_3(O_2CMe)_3L_3] + 3MeCO_2H + 3H^+ + 3e \quad (\mathbf{2}, L = L^1; \mathbf{3}, L = L^2; \mathbf{4}, L = L^3) \quad (1)$$

where Fe^{II} is oxidized to Fe^{III} by oxygen from the air. It is possible to obtain **2** and **4** in crystalline form by recrystallization of the crude product from CH_2Cl_2/hexane, and these complexes were structurally characterized by X-ray diffraction. Although the IR and elemental analysis data confirm

(24) Spek, A. L. *Acta Crystallogr.* **1990**, *A46*, C34.
(25) Wernsdorfer, W. *Adv. Chem. Phys.* **2001**, *118*, 99.
(26) Borrás-Almenar, J. J.; Clemente-Juan, J. M.; Coronado, E.; Tsukerblatt, B. S. MAGPACK. *Inorg. Chem.* **1999**, *38*, 6081.
(27) Spiering, H.; Deák, L.; Bottyán, L. *Hyperfine Interact.* **2000**, *125*, 197.

Scheme 1

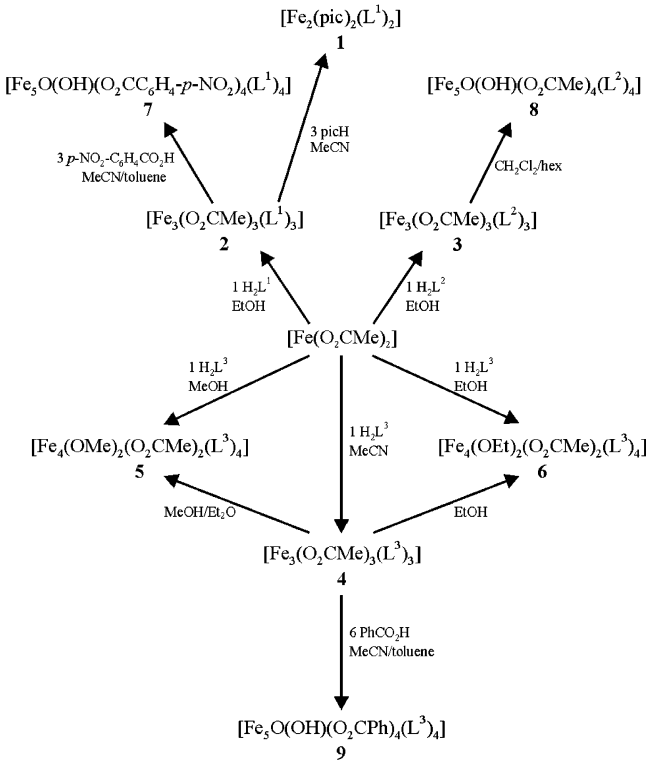

that crude **3** is a similar trinuclear complex, recrystallization of **3** from CH_2Cl_2/hexane affords the pentanuclear complex **8** in high yield:

$$5[Fe_3(O_2CMe)_3(L^2)_3] + 6H_2O \rightarrow 3[Fe_5O(OH)(O_2CMe)_4(L^2)_4] + 3MeCO_2H + 3H_2L^2 \quad (2)$$

The additional oxo and hydroxo ligands in the pentanuclear species apparently result from residual H_2O in the solvent.[28]

A similar treatment of a slurry of $Fe(OAc)_2$ in MeOH or EtOH with 1 equiv of H_2L^3 gives the tetranuclear species **5** and **6**, respectively, according to

$$4Fe(O_2CMe)_2 + 4H_2L^3 + 2ROH \rightarrow [Fe_4(OR)_2(O_2CMe)_2(L^3)_4] + 6MeCO_2H + 4H^+ + 4e \quad (\mathbf{5}, R = Me; \mathbf{6}, R = Et) \quad (3)$$

Alternatively, recrystallization of **4** from MeOH/Et_2O affords crystals of **5** that are suitable for X-ray diffraction, together with a pale amorphous precipitate. Similarly, upon standing, a saturated solution of **4** in EtOH produces tiny single crystals of **6**:

$$4[Fe_3(O_2CMe)_3(L^3)_3] + 6ROH \rightarrow 3[Fe_4(OR)_2(O_2CMe)_2(L^3)_4] + 6MeCO_2H \quad (\mathbf{5}, R = Me; \mathbf{6}, R = Et) \quad (4)$$

However, removal of the precipitate that forms alongside crystals of **5** proved impossible. In addition, crude and crystalline samples of **5** and **6** are insoluble in common organic solvents, which prevented attempts to obtain a pure sample of **5** by further recrystallization. Thus, a pure bulk sample of **5** was not available for elemental analysis or SQUID measurements. In contrast, although crystals of **6** large enough for X-ray characterization could not be obtained, microcrystalline samples are analytically pure and the IR spectrum is essentially identical to that of crystals of **5**, confirming that **6** is the ethoxo analogue of **5**.

Carboxylate exchange was investigated for **2** and **4** in an effort to produce analogous trinuclear complexes with carboxylates other than acetate. A variety of carboxylates were explored; however, it proved difficult to obtain pure species. Nevertheless, reaction of a slurry of **2** in MeCN/toluene with 3 equiv of p-$NO_2C_6H_4CO_2H$, followed by repeated evaporation to dryness and redissolution in toluene to remove the $MeCO_2H$ via the toluene/$MeCO_2H$ azeotrope, affords pentanuclear **7** in reasonable yield. A similar treatment of **4** with 6 equiv of $PhCO_2H$ affords pentanuclear **9**:

$$5[Fe_3(O_2CMe)_3(L)_3] + 12RCO_2H + 6H_2O \rightarrow 3[Fe_5O(OH)(O_2CR)_4(L)_4] + 15MeCO_2H + 3H_2L \quad (\mathbf{7}, L = L^1, R = p\text{-}NO_2C_6H_4; \mathbf{9}, L = L^3, R = Ph) \quad (5)$$

Again the new oxo and hydroxo ligands in the pentanuclear species probably result from residual H_2O in the solvent.[28]

Finally, the reaction of **2** with 3 equiv of picH affords the binuclear species **1** in high yield:

$$2[Fe_3(O_2CMe)_3(L^1)_3] + 6picH \rightarrow 3[Fe_2(pic)_2(L^1)_2] + 6MeCO_2H \quad (6)$$

In this case, although picH possesses a carboxylic acid functionality, pic^- binds in a chelating manner through N and O donor atoms, rather than in a bridging mode through the carboxylate moiety. Presumably, this is due to the greater stability provided to the resulting complex by chelation. It seems likely that reaction of **2** with other simple chelating ligands will result in similar binuclear complexes, although this was not pursued further.

Structure Description. Labeled structural diagrams of the complexes of interest are presented in Figures 1 (**1**), 2 (**2** and **4**), 3 (**5**), and 4 (**7**−**9**). The most relevant interatomic distances and angles are available in Tables 3−5, while more complete listings are available in the Supporting Information (Tables S1−S7).

Complex **1** crystallizes in the monoclinic space group $C2/c$. The asymmetric unit contains half of the molecule of interest together with a disordered CH_2Cl_2 molecule that is 50% occupied. The complex contains a $\{Fe^{III}_2(\mu_2\text{-}O)_2\}^{2+}$ core, where the Fe centers are bridged by the ethoxo-type O atoms from the $(L^1)^{2-}$ ligands (Figure 1). Crystallographic C_2 point symmetry is present, with the C_2 axis passing through the center of the $\{Fe^{III}_2O_2\}^{2+}$ core, coinciding with the crystallographic b axis. The $(L^1)^{2-}$ ligands coordinate in a meridional bischelating fashion, and the remainder of the peripheral ligation is provided by chelating pic^- ligands. The

(28) Aromi, G.; Aubin, S. M. J.; Bolcar, M. A.; Christou, G.; Eppley, H. J.; Folting, K.; Hendrickson, D. N.; Huffman, J. C.; Squire, R. C.; Tsai, H.-L.; Wang, S.; Wemple, M. W. *Polyhedron* **1998**, *17*, 3005 and references therein.

Table 3. Fe−O Distances (Å) for **1**·CH_2Cl_2, **2**·CH_2Cl_2, **4**·CH_2Cl_2, **5**·0.5MeOH, **7**·H_2O·C_7H_8·0.5C_6H_{14}, **8**·0.25H_2O·4.5CH_2Cl_2, and **9**·1.5H_2O·2CH_2Cl_2·0.5C_2H_4O[a]

compd	Fe−O (alkoxo or phenoxo)	Fe−O (hydroxo)	Fe−O (oxo)
1·CH_2Cl_2	1.999(2)−2.028(2)		
2·CH_2Cl_2	1.943(5)−2.057(6)		
4·CH_2Cl_2	1.918(8)−2.026(7)		
5·0.5MeOH	1.965(2)−2.037(2)		
7·H_2O·C_7H_8·0.5C_6H_{14}	1.948(3)−2.096(4)	2.023(3)−2.098(3)	1.879(3)−1.930(3)
8·0.25H_2O·4.5CH_2Cl_2	1.956(5)−2.130(5)	1.987(5)−2.072(4)	1.889(5)−1.937(5)
9·1.5H_2O·2CH_2Cl_2·0.5C_2H_4O	1.981(4)−2.111(4)	2.020(3)−2.103(3)	1.881(4)−1.925(4)

[a] Distances to bridging O atoms only.

Table 4. Fe···Fe Distances (Å) for **1**·CH_2Cl_2, **2**·CH_2Cl_2, **4**·CH_2Cl_2, **5**·0.5MeOH, **7**·H_2O·C_7H_8·0.5C_6H_{14}, **8**·0.25H_2O·4.5CH_2Cl_2, and **9**·1.5H_2O·2CH_2Cl_2·0.5C_2H_4O

compd	via $(\mu\text{-O})_2$[a]	via μ_2-alkoxo	via μ_3-oxo
1·CH_2Cl_2	3.124(2)		
2·CH_2Cl_2		3.409(2)−3.519(2)	
4·CH_2Cl_2		3.409(2)−3.534(2)	
5·0.5MeOH	3.111(2)	3.544(2)	
7·H_2O·C_7H_8·0.5C_6H_{14}	2.989(2)−3.205(2)	3.534(2)−3.555(2)	3.374(2)−3.384(2)
8·0.25H_2O·4.5CH_2Cl_2	3.002(2)−3.218(2)	3.549(2)−3.591(2)	3.357(2)−3.396(2)
9·1.5H_2O·2CH_2Cl_2·0.5C_2H_4O	3.007(2)−3.219(2)	3.532(2)−3.592(2)	3.347(2)−3.388(2)

[a] O may be from oxo, hydroxo, alkoxo, or phenoxo.

Table 5. Fe−O−Fe Bridging Angles (deg) for **1**·CH_2Cl_2, **2**·CH_2Cl_2, **4**·CH_2Cl_2, **5**·0.5MeOH, **7**·H_2O·C_7H_8·0.5C_6H_{14}, **8**·0.25H_2O·4.5CH_2Cl_2, and **9**·1.5H_2O·2CH_2Cl_2·0.5C_2H_4O

compd	via $(\mu\text{-O})_2$[a]	via μ_2-alkoxo	via μ_3-oxo
1·CH_2Cl_2	101.71(6)		
2·CH_2Cl_2		115.4(2)−124.7(2)	
4·CH_2Cl_2		116.1(4)−125.7(4)	
5·0.5MeOH	100.8(1)−102.9(1)	126.5(1)	
7·H_2O·C_7H_8·0.5C_6H_{14}	92.7(1)−104.5(1)	123.6(2)−126.4(2)	124.7(2)−125.9(2)
8·0.25H_2O·4.5CH_2Cl_2	93.7(2)−105.8(2)	125.3(3)−127.9(2)	123.1(2)−126.0(3)
9·1.5H_2O·2CH_2Cl_2·0.5C_2H_4O	92.7(1)−104.4(2)	122.6(2)−126.2(2)	123.1(2)−126.4(2)

[a] O may be from oxo, hydroxo, alkoxo, or phenoxo.

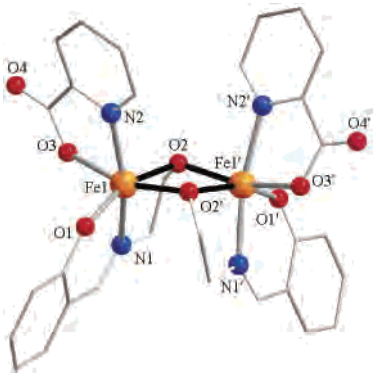

Figure 1. Structure of **1** in **1**·CH_2Cl_2.

noncoordinated O atoms of the pic^- ligands participate in an intermolecular O···H−C hydrogen bond with the C16 atoms of the CH_2Cl_2 molecules of crystallization, with a C···O separation of 3.25 Å.

Complex **2** crystallizes in the orthorhombic space group $Pca2_1$, while complex **4** crystallizes in the monoclinic space group $P2_1/c$. In addition to two molecules of CH_2Cl_2, the asymmetric unit of **2** contains two independent trinuclear complexes with enantiomeric configurations but different interatomic distances and angles. The asymmetric unit of **4** contains a single trinuclear molecule together with one CH_2Cl_2 molecule. All three trinuclear complexes are isostructural, disregarding the differences in the Schiff base ligands. The complexes each possess a $\{Fe^{III}_3(\mu_2\text{-O})_3\}^{3+}$ core, with the three Fe atoms located at the vertexes of a scalene triangle (Figure 2). Each pair of Fe centers is bridged by an ethoxo-type O atom of $(L^1)^{2-}$ or $(L^3)^{2-}$ for **2** and **4**, respectively, in addition to a μ_2-$MeCO_2^-$ ligand. The Schiff base ligands bind in a fashion similar to that observed in **1**. The ligand arrangement is such that two of the core O atoms and one $MeCO_2^-$ ligand lie on one side of the Fe_3 plane, while the third core O atom and the remaining two $MeCO_2^-$ ligands lie on the other. The $\{Fe_3O_3\}^{3+}$ cores and the molecules as a whole all have C_1 point symmetry. Although complexes **2** and **4** are essentially isostructural, inspection of the coordination geometries at the individual Fe sites reveals that **4** is somewhat more distorted than **2**. This can be quantified by a consideration of the variation in Fe−X bond lengths, where Fe1 of **4** displays a variation of 0.31 Å, versus the variation of 0.17−0.22 Å evident in all of the other Fe centers in **2** and **4**. Finally, triangular Fe^{III}_3 clusters and in particular the basic carboxylates $[Fe_3O(O_2CR)_6(X)_3]^+$ (X = e.g., H_2O) are well-known.[29] However, complexes with a $\{Fe_3(\mu_2\text{-O})_3\}^{3+}$ core with alkoxo-type O atoms and no central μ_3-bridge are unknown. There are only two species reported in the literature with the same core topology, one with a $(\mu\text{-oxo})_3$ core and one with $(\mu\text{-hydroxo})(\mu\text{-oxo})_2$.[30,31] Both display no additional ligands bridging the Fe centers.

(29) Cannon, R. D.; White, R. P. *Prog. Inorg. Chem.* **1988**, *36*, 195.

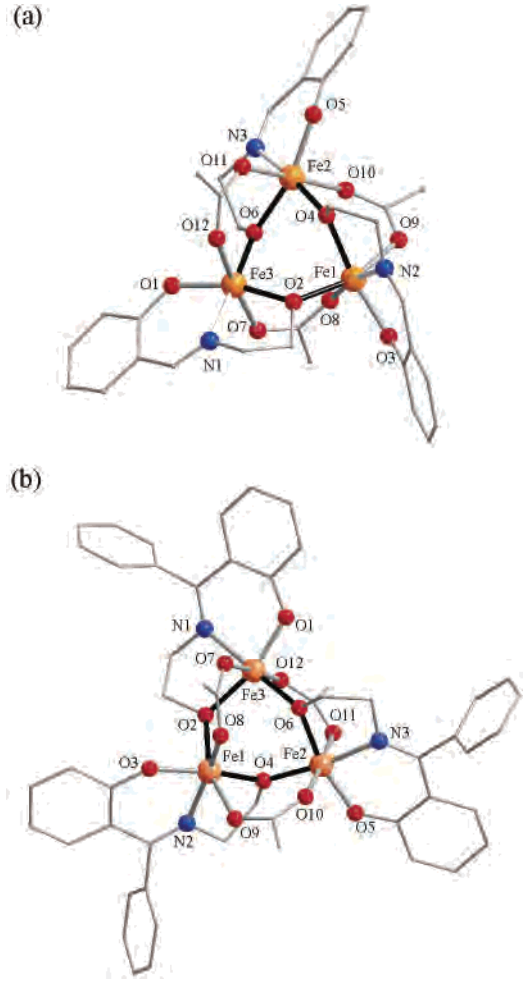

Figure 2. Structure of (a) one of the independent molecules of **2** in **2**·CH_2Cl_2 and (b) **4** in **4**·CH_2Cl_2.

Complex **5** crystallizes in the monoclinic space group $P2/c$. The asymmetric unit contains half of the molecule of interest together with a disordered MeOH molecule that is 25% occupied. The complex contains a $\{Fe^{III}_4(\mu_2\text{-}O)_6\}$ core, where four of the bridging O atoms are ethoxo-type O atoms from $(L^3)^{2-}$ and the other two are from additional μ_2-MeO^- units (Figure 3). The Fe centers are located on the vertexes of a rectangle, such that the sides of the rectangle are alternately encompassed by one or two O atom bridges. The two sides of the rectangle that contain only a single O atom bridge each possess an additional μ_2-$MeCO_2^-$ bridge. This arrangement results in two long (3.5 Å) and two short (3.1 Å) Fe···Fe separations. The $(L^3)^{2-}$ ligands bind in a fashion similar to that observed in **1**, **2,** and **4**. Crystallographic C_2 point symmetry is present, with the C_2 axis passing through the center of the $\{Fe^{III}_4O_4\}^{4+}$ core, coinciding with the crystallographic *a* axis. Although numerous tetranuclear Fe complexes are known,[32] a search of the Cambridge Crystallographic Database reveals that the core evident in **5** is unprecedented in Fe chemistry.

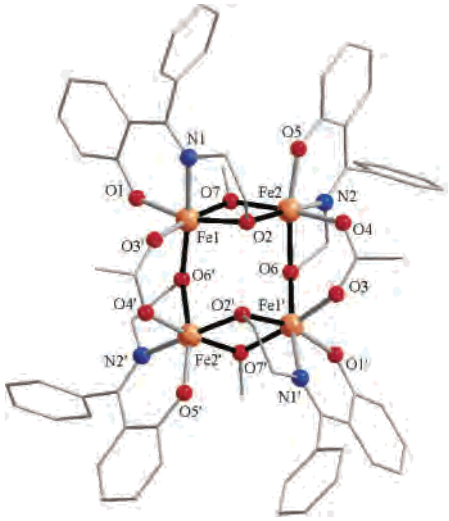

Figure 3. Structure of **5** in **5**·0.5MeOH.

Complexes **7**−**9** all crystallize in the triclinic space group $P\bar{1}$. In addition to disordered solvent, the asymmetric units of **7** and **9** contain one pentanuclear complex, while the asymmetric unit of **8** contains two independent pentanuclear molecules. All three complexes are isostructural, with similar metric parameters and a $\{Fe_5(\mu_3\text{-}O)_2(\mu_2\text{-}O)_5)\}^+$ core (Figure 4). The five (μ_2-O) atoms are from the Schiff base ligands and are ethoxo-type (**7** and **8**, O4, O6, O14, and O16; **9**, O4, O10, O12, and O13) or phenoxo-type (**7** and **8**, O5; **9**, O11), while the μ_3-bridges are oxo (O2) and hydroxo (O1) groups. The core unit has a complex structure that, with some imagination, can be described as an incomplete cubane extended at one face by an incomplete adamantane unit. The four carboxylato ligands provide additional bridges, three binding in the typical μ_2-mode, while the fourth binds in a terminal manner, displaying an intramolecular O···H−O hydrogen bond to the core hydroxo group, with O···O separations of 2.57, 2.55, and 2.57 Å for **7**, **8** and **9**, respectively. Thus, the molecules are unusual in that they contain oxo-, hydroxo- alkoxo-, and carboxylato- bridging units. The peripheral ligation is completed by the Schiff base ligands, with each bound in a fashion similar to that observed in complexes **1**, **2**, **4**, and **5**. However, one Schiff base ligand in each pentanuclear complex possesses a bridging phenoxo-type O atom, which is not observed in the other complexes. The hydroxo H atoms were located crystallographically in all three structures. In addition, bond valence sum calculations are consistent with five Fe^{III} centers for each complex. A search of the Cambridge Crystallographic Database reveals that the core unit evident in **7**−**9** is unprecedented for any pentanuclear complex. Moreover, only three pentanuclear Fe^{III} complexes have been reported previously, all with structures very different from those of **7**−**9**.[33]

Magnetic Studies. Variable-temperature magnetic susceptibility measurements were performed at 0.1 T on powdered crystals of **1**·CH_2Cl_2, **2**, **4**, **6**·H_2O, **7**, **8**·H_2O, and

(30) Zheng, H.; Zang, Y.; Dong, Y.; Young, V. G., Jr.; Que, L., Jr. *J. Am. Chem. Soc.* **1999**, *121*, 2226.
(31) Furutachi, H.; Ohyama, Y.; Tsuchiya, Y.; Hashimoto, K.; Fujinami, S.; Uehara, A.; Suzuki, M.; Maeda, Y. *Chem. Lett.* **2000**, 1132.
(32) Murray, K. S. *Adv. Inorg. Chem.* **1995**, *43*, 261.
(33) (a) Mikuriya, M.; Nakadera, K. *Chem. Lett.* **1995**, 213. (b) Mikuriya, M.; Hashimoto, Y.; Nakashima, S. *Chem. Commun.* **1996**, 295. (c) O'Keefe, B. J.; Monnier, S. M.; Hillmeyer, M. A.; Tolman, W. B. *J. Am. Chem. Soc.* **2001**, *123*, 339.

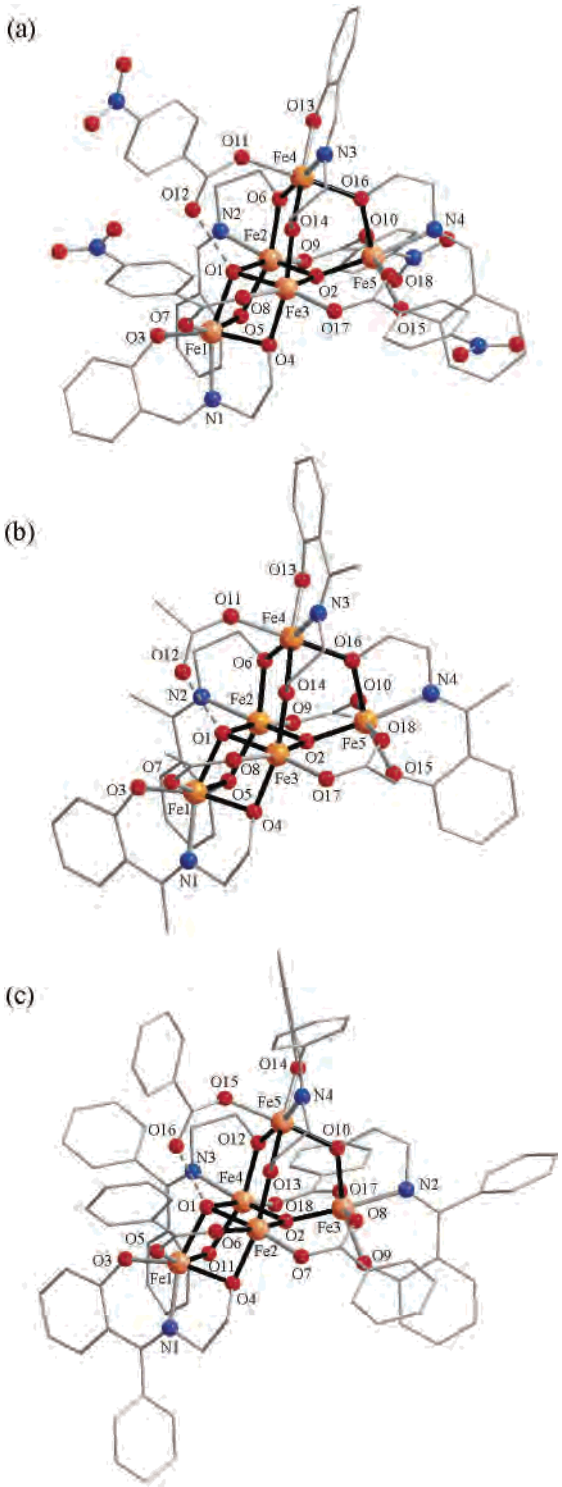

Figure 4. Structure of (a) **7** in **7**·H_2O·C_7H_8·0.5C_6H_{14}, (b) one of the independent molecules of **8** in **8**·0.25H_2O·4.5CH_2Cl_2, and (c) **9** in **9**·1.5H_2O·2CH_2Cl_2·0.5C_2H_4O.

9·2H_2O, in the temperature range 1.8−300 K. The data for **1**·CH_2Cl_2, **2**, **6**·H_2O, and **8**·H_2O are plotted in Figures 5, 6a, 7a, and 8a, respectively, as $\chi_M T$ vs T and χ_M vs T, together with the fits of the experimental data. The data for **4**, **7**, and **9**·2H_2O are available in Figures S1, S2, and S3, respectively.

For **1**·CH_2Cl_2 (Figure 5), $\chi_M T$ at 300 K is ∼7.0 cm^3 mol^{-1} K, which is less than the calculated spin-only value of 8.8 cm^3 mol^{-1} K for two noninteracting Fe^{III} centers with g =

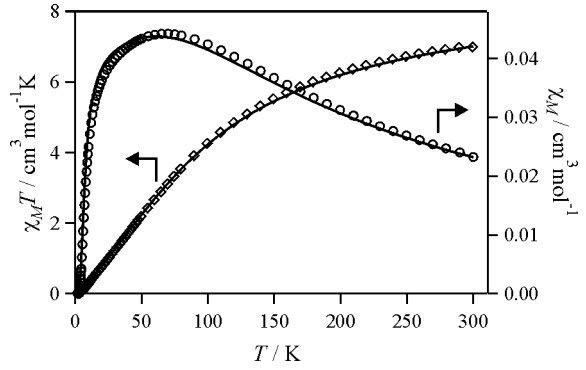

Figure 5. $\chi_M T$ (◇) and χ_M (○) vs T for **1**·CH_2Cl_2. The solid lines are fits as described in the text.

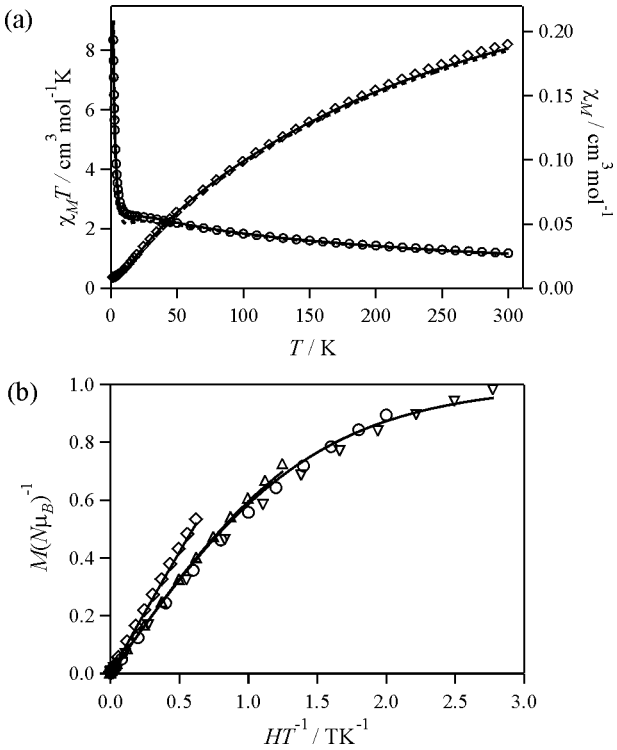

Figure 6. Magnetic data for **2**: (a) $\chi_M T$ (◇) and χ_M (○) vs T and (b) $M(N\mu_B)^{-1}$ vs HT^{-1} at 1.8 (▽), 2.5 (○), 4 (△), and 8 K (◇). The solid lines are fits or simulations of the magnetic susceptibility or magnetization data as described in the text. The dashed lines in (a) are the simulations of the susceptibility data calculated using the parameters derived from INS measurements (see the text).

2.0, suggesting an antiferromagnetic interaction. As the temperature is decreased to 1.8 K, $\chi_M T$ decreases steadily to ∼0 cm^3 mol^{-1} K, consistent with an $S = 0$ ground state. To determine the magnitude of the exchange interaction, the susceptibility data were fit with g fixed to 2.0 to the exchange Hamiltonian

$$\hat{H}_{ex} = -2J(\mathbf{S}_A \cdot \mathbf{S}_B) \qquad (7)$$

yielding $J = -7.3(2)$ cm^{-1}.

For **2** (Figure 6a) and **4** (Figure S1a), the value of $\chi_M T$ at 300 K is ∼8.2 cm^3 mol^{-1} K, which is significantly less than the calculated spin-only value of 13.1 cm^3 mol^{-1} K for three noninteracting Fe^{III} centers with g = 2.0. This and the decrease in $\chi_M T$ as the temperature is decreased are consistent with overall antiferromagnetic interactions in the molecule.

The values of $\chi_M T$ at 1.8 K are ~0.35 $cm^3\ mol^{-1}\ K$, suggesting $S = 1/2$ ground states (for an $S = 1/2$ system with $g = 2.0$, $\chi_M T$ is calculated to be 0.38 $cm^3\ mol^{-1}\ K$ at 0 K). Crystallographically, the three Fe centers in complexes **2** and **4** are arranged at the vertexes of a scalene triangle, resulting in the coupling scheme presented in Chart 2.

Chart 2

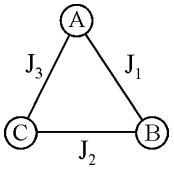

The data were fit with g fixed to 2.0 to the exchange Hamiltonian

$$\hat{H}_{ex} = -2J_1(\mathbf{S}_A \cdot \mathbf{S}_B) - 2J_2(\mathbf{S}_B \cdot \mathbf{S}_C) - 2J_3(\mathbf{S}_A \cdot \mathbf{S}_C) \quad (8)$$

yielding $J_1 = -10.4(9)\ cm^{-1}$, $J_2 = -9.4(7)\ cm^{-1}$, and $J_3 = -8.6(4)\ cm^{-1}$ for **2** and $J_1 = -10.7(4)\ cm^{-1}$, $J_2 = -10.1(4)\ cm^{-1}$, and $J_3 = -9.0(3)\ cm^{-1}$ for **4**. For both compounds, the three competing antiferromagnetic interactions result in a spin-frustrated system and an $S = 1/2$ ground state. It was found that a significant improvement was obtained in the fit using three different exchange parameters rather than one or two, which is in agreement with the inequivalence of the three metal centers observed in the X-ray structures. The similarity between the three coupling constants determined for each complex is consistent with the similarity between the three Fe···Fe bridging geometries evident in the structures; however, this similarity precludes the assignment of particular coupling constants to particular pairwise interactions. In addition, the set of parameters determined for the two complexes are the same within experimental error, which is consistent with the similarity in the core topologies and metric parameters. Finally, it is relevant to the discussion of inelastic neutron scattering studies that follows to note that the J values derived for **2** imply an $S = 1/2$ excited state at 9.4 cm^{-1} above the $S = 1/2$ ground state and four $S = 3/2$ excited states at 19−48 cm^{-1} above the ground state. A similar arrangement of energy levels is implied for **4**.

Variable-temperature magnetization measurements were performed on **2** and **4** in the temperature range 1.8−8 K, with fields up to 5 T. The data for **2** are presented in Figure 6b as plots of $M(N\mu_B)^{-1}$ vs HT^{-1}, while the data for **4** are available in Figure S1b. For both species, the $M(N\mu_B)^{-1}$ values at 5 T and 1.8 K of 0.98 and 0.93 for **2** and **4**, respectively, are consistent with $S = 1/2$ ground states. It is possible to reproduce the magnetization data for **2** using the parameters determined from the fit of the susceptibility data (Figure 6b). The simulation of the data for **4** is slightly less satisfactory, which may be due to the presence of intermolecular interactions.

For **6**·H_2O (Figure 7), the value of $\chi_M T$ at 300 K is ~10.3 $cm^3\ mol^{-1}\ K$, which is substantially less than the calculated spin-only value of 17.5 $cm^3\ mol^{-1}\ K$ for four noninteracting Fe^{III} centers with $g = 2.0$. Again the behavior suggests overall antiferromagnetic interactions, with $\chi_M T$ decreasing steadily

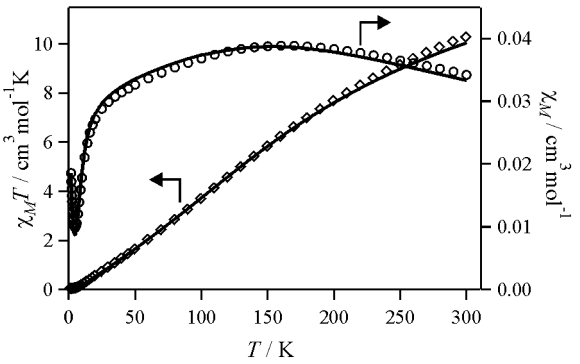

Figure 7. $\chi_M T$ (◇) and χ_M (○) vs T for **6**·H_2O. The solid line is the sum of the fits of the low-temperature data and the high-temperature data as described in the text.

to a value of ~0 $cm^3\ mol^{-1}\ K$ at 1.8 K, consistent with an $S = 0$ ground state. Correspondingly, χ_M increases gradually before reaching a broad maximum at about 150 K and decreasing gradually as the temperature is decreased to 4.5 K. Below 4.5 K, χ_M increases rapidly as the temperature is decreased, which is attributed to the presence of a paramagnetic impurity. Fitting the data below 4.5 K to the Curie law suggests 0.19 mol % monomeric Fe^{III} impurity. Crystallographically, the four Fe centers in complex **5** (and presumably **6**) are arranged at the vertexes of a rectangle, resulting in the coupling scheme presented in Chart 3.

Chart 3

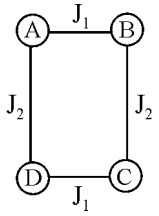

The data were scaled to correct for the monomeric impurity, and the data above 10 K were fit with g fixed to 2.0 to the exchange Hamiltonian

$$\hat{H}_{ex} = -2J_1(\mathbf{S}_A \cdot \mathbf{S}_B + \mathbf{S}_C \cdot \mathbf{S}_D) - 2J_2(\mathbf{S}_B \cdot \mathbf{S}_C + \mathbf{S}_A \cdot \mathbf{S}_D) \quad (9)$$

yielding the set of parameters $J_1 = -9.2(2)\ cm^{-1}$ and $J_2 = -10.2(4)\ cm^{-1}$, which result in an $S = 0$ ground state. A second set of parameters with $J_1 > 0$ was found to reproduce the data equally well, but was rejected because antiferromagnetic coupling is typically observed for ferric complexes with bridging geometries similar to those evident in **5** (and presumably **6**).[34,35] Although it was found that a significant improvement was obtained in the fit using two different exchange parameters rather than only one, the similarity in

(34) (a) Kato, M.; Yamada, Y.; Inagaki, T.; Mori, W.; Sakai, K.; Tsubomura, T.; Sato, M.; Yano, S. *Inorg. Chem.* **1995**, *34*, 2645 and references therein. (b) Neves, A.; de Brito, M. A.; Vencato, I.; Drago, V.; Griesar, K.; Haase, W. *Inorg. Chem.* **1996**, *35*, 2360 and references therein.

(35) (a) Chiari, B.; Piovesana, O.; Tarantelli, T.; Zanazzi, P. F. *Inorg. Chem.* **1984**, *23*, 3398. (b) Ménage, S.; Que Jr, L. *Inorg. Chem.* **1990**, *29*, 4293 and references therein. (c) Taft, K. L.; Delfs, C. D.; Papaefthymiou, G. C.; Foner, S.; Gatteschi, D.; Lippard, S. J. *J. Am. Chem. Soc.* **1994**, *116*, 823. (d) Raptopoulou, C. P.; Tangoulis, V.; Devlin, E. *Angew. Chem., Int. Ed.* **2002**, *41*, 2386.

the magnitudes of J_1 and J_2 precludes their individual assignment to the two distinct pairwise interactions.

For **7**, **8**·H_2O, and **9**·$2H_2O$ (Figures S2a, 7a, and S3a, respectively), the value of $\chi_M T$ at 300 K is ~10 $cm^3\ mol^{-1}$ K, which is considerably less than the calculated spin-only value of 22 $cm^3\ mol^{-1}$ K for five noninteracting Fe^{III} centers with $g = 2.0$. This and the decrease in $\chi_M T$ as the temperature is decreased are consistent with overall antiferromagnetic interactions. For the three compounds $\chi_M T$ decreases steadily to ~4.3 $cm^3\ mol^{-1}$ K at 35 K, where it levels out before finally decreasing rapidly below 5 K. This suggests a spin ground state of $S = 5/2$ (for an $S = 5/2$ system with $g = 2.0$, $\chi_M T$ is calculated to be 4.4 $cm^3\ mol^{-1}$ K at 0 K). The low-temperature decrease in $\chi_M T$ is assigned to the effects of zero-field splitting (ZFS) and/or antiferromagnetic intermolecular interactions. A consideration of the topologies of the complexes affords the coupling scheme depicted in Chart 4.

Chart 4

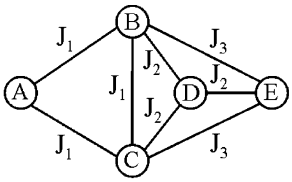

7 and **8**: A = Fe1, B = Fe2, C = Fe3, D = Fe4, E = Fe5
9: A = Fe1, B = Fe4, C = Fe2, D = Fe5, E = Fe3

On the basis of the nature of the Fe−O−Fe bonds, the eight coupling constants that are strictly required can be reduced to three, where J_1 characterizes couplings through a (μ-O)$_2$ unit with Fe−O−Fe angles <106° and Fe···Fe distances of 2.9−3.3 Å, J_2 characterizes couplings through a single μ_2-alkoxo bridge with Fe−O−Fe angles of 123−128° and Fe···Fe distances of 3.5−3.6 Å, and J_3 characterizes couplings through a μ_3-oxo bridge with Fe−O−Fe angles of 123−127° and Fe···Fe distances of 3.3−3.4 Å (Tables 4 and 5). The χ_M and $\chi_M T$ vs T data above 10 K were fit with g fixed to 2.0 to the exchange Hamiltonian

$$\hat{H}_{ex} = -2J_1(\mathbf{S}_A\cdot\mathbf{S}_B + \mathbf{S}_A\cdot\mathbf{S}_C + \mathbf{S}_B\cdot\mathbf{S}_C) - 2J_2(\mathbf{S}_B\cdot\mathbf{S}_D + \mathbf{S}_C\cdot\mathbf{S}_D + \mathbf{S}_D\cdot\mathbf{S}_E) - 2J_3(\mathbf{S}_B\cdot\mathbf{S}_E + \mathbf{S}_C\cdot\mathbf{S}_E) \quad (10)$$

yielding the parameters $J_1 = -3.0(3)$ cm^{-1}, $J_2 = -11.4(6)$ cm^{-1}, and $J_3 = -46(1)$ cm^{-1} for **7**, $J_1 = -3.5(3)$ cm^{-1}, $J_2 = -12.6(5)$ cm^{-1}, and $J_3 = -53(5)$ cm^{-1} for **8**·H_2O, and $J_1 = -2.2(3)$ cm^{-1}, $J_2 = -12.3(5)$ cm^{-1}, and $J_3 = -36(2)$ cm^{-1} for **9**·$2H_2O$. Each set of parameters results in an overall ground state of $S = 5/2$ for the three complexes. A second set of parameters with J_2, $J_3 < 0$ and $|J_2| > |J_3|$ was found to reproduce the data equally well for the three complexes, but was rejected because it has generally been observed that μ-oxo bridges (characterized by J_3) mediate stronger antiferromagnetic interactions than μ-alkoxo bridges (characterized by J_2).[34] In addition, attempts to fit the data using only two coupling constants, assuming that $J_2 = J_3$, gave a significantly poorer fit, while efforts to fit the data using more than three coupling constants were not pursued due to the adequacy of the fit already obtained and the desire to avoid overparametrization. The sets of parameters determined for the three complexes are very similar, which is consistent with the similarity in the core topologies and metric parameters.

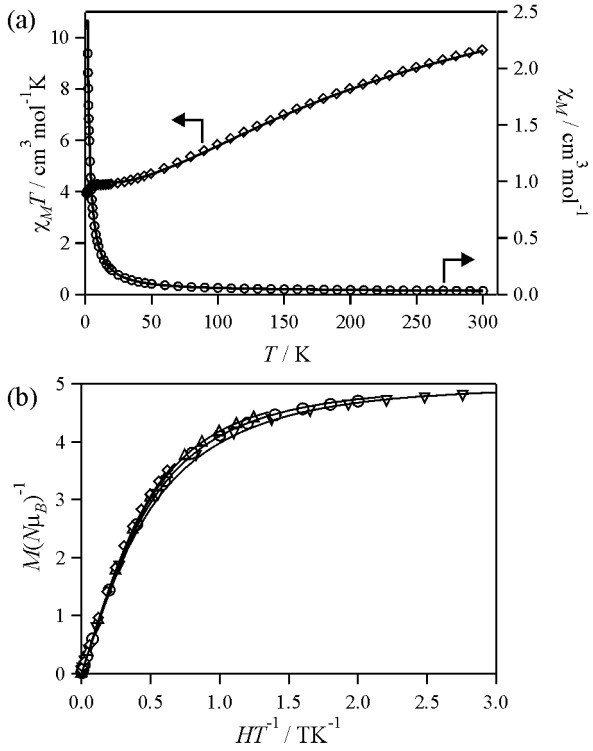

Figure 8. Magnetic data for **8**·H_2O: (a) $\chi_M T$ (◇) and χ_M (○) vs T and (b) $M(N\mu_B)^{-1}$ vs HT^{-1} at 1.8 (▽), 2.5 (○), 4 (△), and 8 K (◇). The solid lines are fits or simulations as described in the text.

Variable-temperature magnetization measurements were performed on **7**, **8**·H_2O, and **9**·$2H_2O$ in the temperature range 1.8−8 K, with fields up to 5 T. The data for **8**·H_2O are presented in Figure 8b as plots of $M(N\mu_B)^{-1}$ vs HT^{-1}, while the data for **7** and **9**·$2H_2O$ are available in Figures S2b and S3b, respectively. For the three species, the $M(N\mu_B)^{-1}$ values of ~4.8 at 5 T and 1.8 K are consistent with $S = 5/2$ ground states. In each case the data deviate slightly from the Brillouin function for $S = 5/2$. This deviation can be reproduced upon the incorporation of an axial ZFS term, D, and it is possible to simulate the data using the ZFS Hamiltonian

$$\hat{H}_{ZFS} = D(\hat{S}_z^2 - S(S+1)/3) \quad (11)$$

assuming axial anisotropy and a well-isolated $S = 5/2$ ground state. Two sets of simulation parameters have been determined for each compound that reproduce the data equally well: $g = 1.99(1)$ and $D = -0.46(3)$ or $0.59(2)$ cm^{-1} for **7**, $g = 1.99(1)$ and $D = -0.45(3)$ or $0.52(4)$ cm^{-1} for **8**·H_2O, and $g = 2.01(1)$ and $D = -0.35(2)$ or $0.42(2)$ cm^{-1} for **9**·$2H_2O$.

In an effort to determine which parameter set obtained from the magnetization fits is correct and whether the D

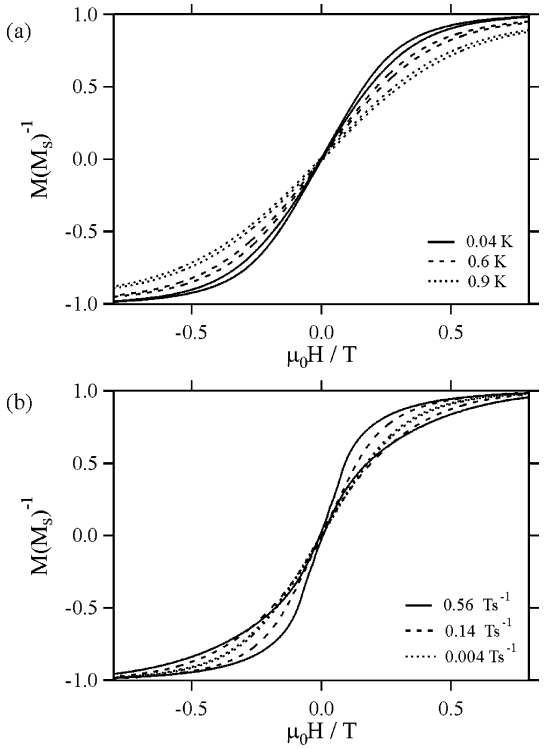

Figure 9. Magnetization hysteresis loops for a single crystal of **8**·$0.25H_2O$·$4.5CH_2Cl_2$ measured parallel to the easy axis (a) with a scan rate of 0.035 T s^{-1} and different temperatures and (b) at 0.04 K and different scan rates.

parameter for the pentanuclear complexes is positive or negative, low-temperature magnetization measurements were performed on single crystals of **8**·$0.25H_2O$·$4.5CH_2Cl_2$ down to 0.04 K using a micro-SQUID apparatus. If $D < 0$, the $S = 5/2$ and $D = -0.45$ cm^{-1} values suggest that **8** should have an anisotropy barrier to magnetization reversal of $(S^2 - 1/4)|D| \approx 2.7$ cm^{-1}. This is potentially large enough for the manifestation of slow relaxation of the magnetization below 1 K. Figure 9 shows magnetization vs field measurements parallel to the experimentally observed easy axis and with the magnetization normalized to the saturation value M_s. First, the experimental observation of an easy axis is consistent with $D < 0$. In addition, at low temperatures hysteresis loops are observed at nonzero magnetic fields whose coercivity increases with decreasing temperature (Figure 9a). Detailed investigations of the dependence of the hysteresis loops on the sweep rate establish that this hysteresis is not only due to a phonon bottleneck, where the phonon exchange (thermal coupling) between the crystal and its environment is retarded, hampering the spin relaxation,[36] but also due to slow relaxation of the magnetization consistent with a molecular anisotropy barrier and $D < 0$. However, the size of the barrier is small, and a reliable Arrhenius plot cannot be obtained. The absence of hysteresis at zero field is often observed for systems with relatively low spin ground states and can be attributed to the presence of rapid quantum tunneling.[12] Despite the fact that theoretically half-integer spin systems should not tunnel in zero field,

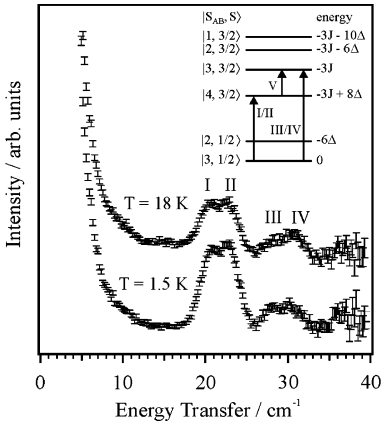

Figure 10. Energy-loss INS spectra of **2** at two temperatures. $\lambda = 3.8$ Å, and the total Q range is from 0.5 to 2.6 $Å^{-1}$. Inelastic focusing is at an energy transfer of 27.5 cm^{-1} with an instrumental resolution of 1.6 cm^{-1}. The labels of the peaks are given in Table 6. The inset shows the corresponding energy level and transition diagram based on an isosceles triangle with $J_1 = J_2 = J$ and $\Delta = J - J_3 < 0$.

Table 6. Observed Transition Energies from the INS Spectra of **2**

label	energy (cm^{-1})	label	energy (cm^{-1})
I	20.4(3)	IV	30.2(3)
II	22.9(3)	V	7.7(3)
III	27.8(3)		

tunneling is generally observed due to coupling with the environment through intermolecular dipolar coupling, hyperfine coupling, spin−spin cross relaxation, and other processes.[11,12,37]

Inelastic Neutron Scattering Studies. INS has previously proved to be a useful tool for the elucidation of the exchange coupling in trinuclear Fe complexes with triangular arrangements of the Fe centers, providing data that are complementary to those obtained from magnetic susceptibility measurements.[38] For compound **2** the energy levels derived from the fit of the magnetic susceptibility data are such that transitions between these levels should be of an energy whose magnitude is suitable for detection by INS. Figure 10 shows the INS spectra of **2** at 1.5 and 18 K, corresponding to the sum of all of the available detectors, i.e., the total Q range from 0.5 and 2.6 $Å^{-1}$. At 1.5 K a pair of peaks centered at around 21.6 cm^{-1} (Table 6) is observed, together with a pair of peaks centered at around 29.0 cm^{-1} (less intense). At 18 K, the intensity of the pair of peaks at 21.6 cm^{-1} is reduced whereas the intensity of the pair of peaks at 29.0 cm^{-1} is essentially unchanged. These peaks are also observed on the energy gain side. The Q dependence (not shown) is consistent with both pairs of peaks arising from magnetic transitions.

In modeling the data the molecular states are labeled as $|S_{AB}, S\rangle$, with the intermediate spin $\vec{S}_{AB} = \vec{S}_A + \vec{S}_B$ and total spin $\vec{S} = \vec{S}_{AB} + \vec{S}_C$ (Chart 2). Calculations using the J values

(36) Chiorescu, I.; Wernsdorfer, W.; Müller, A.; Bogge, H.; Barbara, B. *Phys. Rev. Lett.* **2000**, *84*, 3454.

(37) Boskovic, C.; Wernsdorfer, W.; Folting, K.; Huffman, J. C.; Hendrickson, D. N.; Christou, G. *Inorg. Chem.* **2002**, *41*, 5107.

(38) (a) Furrer, A.; Güdel, H. U. *Helv. Phys. Acta* **1977**, *50*, 439. (b) Cannon, R. D.; Jayasooriya, U. A.; Wu, R.; arapKoske, S. K.; Stride, J. A.; Nielson, O. F.; White, R. P.; Kearley, G. J.; Summerfield, D. *J. Am. Chem. Soc.* **1994**, *116*, 11869. (c) Sowrey, F. E.; Tilford, C.; Wocadlo, S.; Anson, C. E.; Powell, A. K.; Bennington, S. M.; Montfrooij, W.; Jayasooriya, U. A. Cannon, R. D. *J. Chem. Soc., Dalton Trans.* **2001**, 862.

determined from the fit of the susceptibility data for **2** and eq 8 predict INS transitions to and from the $|3, 1/2\rangle$ ground state at 19.4 cm^{-1} ($|3, 1/2\rangle \leftrightarrow |4, 3/2\rangle$) and 28.2 cm^{-1} ($|3, 1/2\rangle \leftrightarrow |3, 3/2\rangle$). INS peaks are observed at roughly these positions and have been assigned accordingly. However, each of these transitions occurs as a pair of peaks, the first as I and II and the second as III and IV. This may be attributed to the presence of two species in the sample, and indeed two independent molecules with different metric parameters were observed in the asymmetric unit in the single-crystal X-ray structure (vide supra). Thus, INS, being a spectroscopic technique, allows the two inequivalent complexes to be distinguished, and the INS data were modeled assuming two species. To avoid overparametrization, the observation of only two peaks per complex requires the use of an isosceles triangular model (Chart 2 and eq 8, $J_1 = J_2 = J$), rather than the scalene model used for the susceptibility data. The energy level diagram for such an antiferromagnetically coupled isosceles triangle is given in the inset of Figure 10, together with the peak assignment. Peaks I and III (Table 6) are assigned to one species, while peaks II and IV belong to the other species. A hot transition V (not shown) is clearly observed at 7.7 cm^{-1} in a high-resolution spectrum. It corresponds to the $|3, 3/2\rangle \leftrightarrow |4, 3/2\rangle$ transitions in both isomers. The parameters which give the best simulation of both the INS and susceptibility data are $J_1 = J_2 = -9.27$ cm^{-1} and $J_3 = -8.34$ cm^{-1} for one isomer and $J_1 = J_2 = -10.08$ cm^{-1} and $J_3 = -9.16$ cm^{-1} for the second isomer. Simulations of the magnetic susceptibility data using these parameters are presented in Figure 6a and reproduce the experimental data very well.

Mössbauer Spectroscopy. ^{57}Fe Mössbauer spectra for compounds **2**, **4**, **7**, and **8**·H_2O were recorded at several temperatures in the range 4.2−293 K, and an additional spectrum was acquired for **8**·H_2O at 1.7 K. The spectra obtained at temperatures >100 K (and at 4.2 K for **2**) were least-squares fit to Lorentzian lines assuming equal contributions from three (**2** and **4**) or five (**7** and **8**·H_2O) Fe sites to give the parameters presented in Table 7. These isomer shift (δ) and quadrupole splitting (ΔE_q) parameters are consistent with the presence of only high-spin Fe^{III} centers.[39] The isomer shift values are observed to decrease with increasing temperature due to the second-order Doppler effect. The spectra obtained at temperatures <100 K were not fitted for **4**, **7**, and **8**·H_2O because of the increase in line width and loss of resolution observed.

The spectra for **2** (Figure 11) and **4** (Figure S4) are consistent with three overlapping quadrupole-split doublets over the temperature range 4.2−293 K. The fitting parameters for both **2** and **4** characterize three ferric sites in each complex with similar δ values. For **2**, the three sites possess three distinct ΔE_q values. The ΔE_q values reflect the deviation from octahedral coordination geometry at each site, with larger ΔE_q values associated with a less symmetric environment. Inspection of the X-ray structural data for **2**·CH_2Cl_2 reveals similar NO_5 coordination environments for all six Fe centers (two independent molecules), with little variation in Fe−X bond lengths (from 0.17 to 0.21 Å). As a result, assignment of the three sites to particular Fe centers is not possible. However, as the X-ray and Mössbauer measurements were performed on differently solvated species, the metric parameters determined crystallographically may differ from those present in the desolvated form that was measured by Mössbauer spectroscopy. For **4**, two of the sites (**4**a and **4**b) have relatively similar ΔE_q values, while **4**c has a significantly larger value of ΔE_q. Inspection of the X-ray structural data for **4**·CH_2Cl_2 reveals that although all three Fe centers have similar NO_5 coordination environments, Fe1 shows a significantly greater variation in Fe−X bond lengths (0.31 Å) than either Fe2 (0.22 Å) or Fe3 (0.19 Å). Although again the X-ray and Mössbauer measurements were performed on differently solvated forms, the data are consistent with the assignment of site **4**c to Fe1, while the specific assignment of the other two sites remains elusive.

The spectra for **7** (Figure S5) and **8**·H_2O (Figure 12) are consistent with five overlapping quadrupole-split doublets, which are better resolved for **8**·H_2O than for **7**. The fitting parameters for **7** and **8**·H_2O characterize five ferric sites with similar δ values. For **7** the ΔE_q values of the five sites lie in

Table 7. Mössbauer Parameters for **2**, **4**, **7**, and **8**·H_2O

compd site	T (K)	δ (mm s^{-1})	ΔE_q (mm s^{-1})	Γ^a
2a	293	0.45	0.49	0.38
	135	0.53	0.52	0.30
	4.2	0.55	0.52	0.29
2b	293	0.42	0.79	0.38
	135	0.51	0.80	0.30
	4.2	0.59	0.93	0.29
2c	293	0.42	1.12	0.38
	135	0.49	1.11	0.30
	4.2	0.46	1.05	0.29
4a	293	0.42	0.72	0.36
	140	0.48	0.77	0.30
4b	293	0.42	0.87	0.36
	140	0.49	0.92	0.30
4c	293	0.41	1.32	0.36
	140	0.46	1.35	0.30
7a	293	0.41	0.49	0.33
	110	0.48	0.58	0.33
7b	293	0.39	0.74	0.33
	110	0.45	0.73	0.33
7c	293	0.40	0.79	0.33
	110	0.51	0.74	0.33
7d	293	0.43	1.37	0.33
	110	0.50	1.40	0.33
7e	293	0.43	1.83	0.33
	110	0.52	1.89	0.33
8a	293	0.42	0.45	0.34
	170	0.46	0.48	0.30
	110	0.49	0.47	0.29
8b	293	0.41	0.70	0.34
	170	0.46	0.71	0.30
	110	0.49	0.69	0.29
8c	293	0.42	0.72	0.34
	170	0.45	0.74	0.30
	110	0.47	0.72	0.29
8d	293	0.43	1.48	0.34
	170	0.46	1.53	0.30
	110	0.47	1.49	0.29
8e	293	0.40	1.66	0.34
	170	0.46	1.72	0.30
	110	0.50	1.75	0.29

[a] Width at half-height.

(39) Murray, K. S. *Coord. Chem. Rev.* **1974**, *12*, 1.

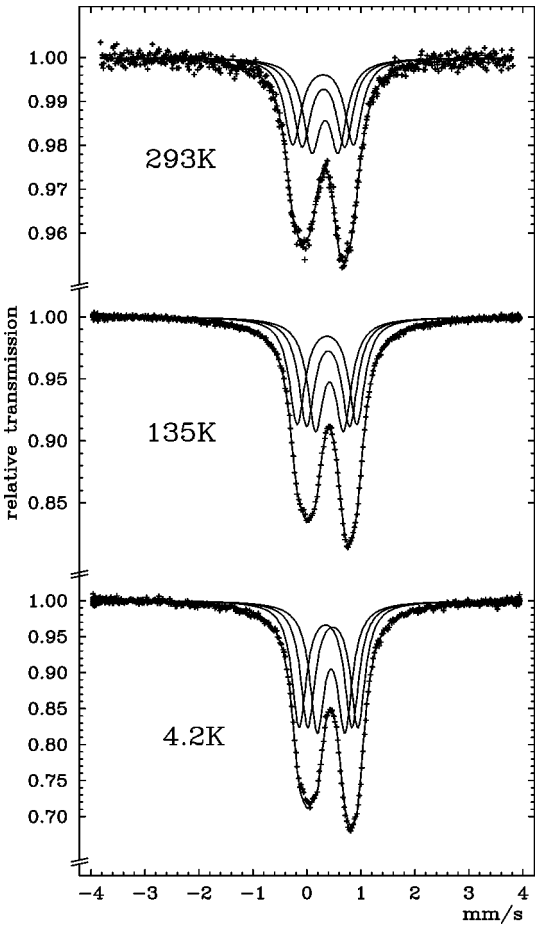

Figure 11. Variable-temperature Mössbauer spectra for **2**. The solid lines are the fits as described in the text.

the order **7**a < **7**b, **7**c < **7**d < **7**e. The variations in Fe−X bond lengths derived from the X-ray structure for **7**·H_2O·C_7H_8·0.5C_6H_{14} are (Fe1) 0.23 Å, (Fe2) 0.18 Å, (Fe3) 0.17 Å, (Fe4) 0.22 Å, and (Fe5) 0.23 Å, with NO_5 coordination environments for all but Fe3, which has O_6 coordination. This is consistent with the tentative assignments **7**a = Fe3, **7**b = Fe2, **7**c = Fe4, and **7**d, **7**e = Fe1, Fe5. For **8**·H_2O the five sites can be broadly classified into three groups on the basis of the ΔE_q values, which lie in the order **8**a < **8**b, **8**c < **8**d, **8**e. The variations in Fe−X bond lengths derived from the X-ray structure for **8**·0.25H_2O·4.5CH_2Cl_2 are (Fe1) 0.23 Å, (Fe2) 0.22 Å, (Fe3) 0.17 Å, (Fe4) 0.26 Å, and (Fe5) 0.27 Å, with the same coordination environments as **7**. This suggests the assignments **8**a = Fe3, **8**b, **8**c = Fe1, Fe2, and **8**d, **8**e = Fe4, Fe5. However, again the X-ray and Mössbauer measurements were performed on differently solvated forms of **7** and **8**, whose metric parameters may differ slightly. Hence, the assignments are not unequivocal, although the trends between the structural and Mössbauer data correlate better for **8** than for **7**.

The spectra for both **7** and **8**·H_2O broaden as the temperature is decreased to 4.2 K, displaying a deviation from the theoretical Lorentzian line shape. This is characteristic of a decrease in the spin flip frequency, and as a result the data below 110 K were not fitted. Curiously, the spectrum of **8**·H_2O at 1.7 K displays a sharpening of the lines; however, the origin of this is uncertain. Additional

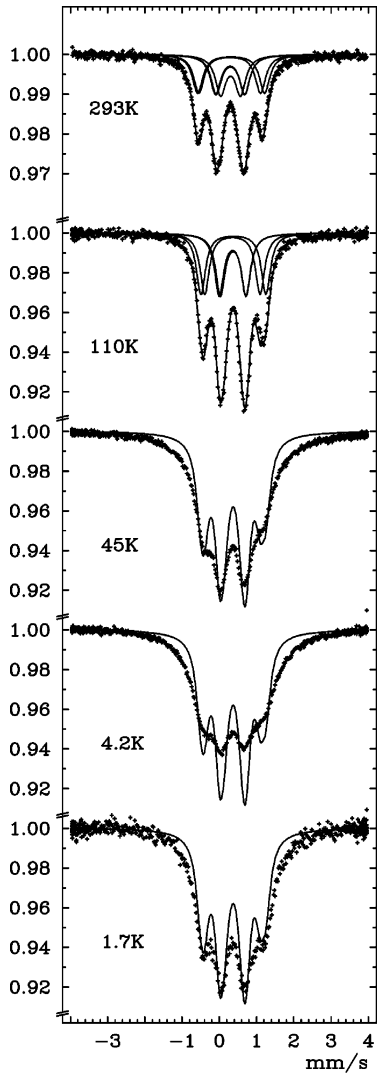

Figure 12. Variable-temperature Mössbauer spectra for **8**·H_2O. For temperatures above 100 K the solid lines are the fits as described in the text. For the lower temperatures the solid lines correspond to the theoretical spectra derived from the fitting parameters for the 110 K data.

measurements in the presence of a magnetic field would be required to determine the nature of the complex relaxation effects which give rise to this behavior. Finally, even down to 1.7 K the spectrum of **8**·H_2O shows no magnetic splitting due to slow magnetization relaxation associated with an anisotropy barrier.

Discussion

The values derived from the fits of the magnetic susceptibility data for the magnetic exchange interactions for compounds **1**·CH_2Cl_2, **2, 4**, **6**·H_2O, **7**, **8**·H_2O, and **9**·2H_2O are presented in Table 8, where the carboxylato bridges are ignored for the purposes of categorizing the interactions. With the exception of **6**·H_2O, these coupling constants can all be assigned to particular superexchange pathways. For **6**·H_2O the similarity in the J values of the two coupling constants precludes their specific assignment to the two different bridging units evident in the structure. All of the determined coupling constants are antiferromagnetic, which

Table 8. J (cm^{-1}) Determined for Compounds **1**·CH_2Cl_2, **2**, **4**, **6**·H_2O, **7**, **8**·H_2O, and **9**·$2H_2O$

compd	via $(\mu\text{-O})_2$[a]	via μ_2-alkoxo	via μ_3-oxo	P[b]
1·CH_2Cl_2	−7.3(2)			2.01
2		−8.6(4), −9.4(7), −10.4(9)		1.98, 2.00, 2.02
4		−9.0(3), −10.1(4), −10.7(4)		1.97, 1.99, 2.01
6·H_2O	−9.2(2) or −10.2(4)[c]	−9.2(2) or −10.2(4)[c]		1.98, 1.99
7	−3.0(3)	−11.4(6)	−46(1)	1.90[d]
8·H_2O	−3.5(3)	−12.6(5)	−53(5)	1.91[d]
9·$2H_2O$	−2.2(3)	−12.3(5)	−36(2)	1.90[d]

[a] O may be from oxo, hydroxo, alkoxo, or phenoxo. [b] Defined in ref 40. [c] The asignment of one value to $(\mu\text{-O})_2$ and one to μ_2-alkoxo is uncertain. [d] Only applicable for the exchange interaction via μ_3-oxo.

is typical for these types of superexchange pathways.[4,34,35] Gorun and Lippard have determined an empirical correlation between J (cm^{-1}) and the parameter P (Å), which is the shortest superexchange pathway defined as the shortest distance between the metal(s) and the bridging ligand(s), for pairs of doubly or triply bridged high-spin Fe^{III} centers:[40]

$$-J = (8.763 \times 10^{11})\exp(-12.663P) \qquad (12)$$

The value of P has been calculated, where applicable, for the present complexes and included in Table 8. P has not been calculated for two of the three interactions for the pentanuclear complexes **7**, **8**·H_2O, and **9**·$2H_2O$, because as an approximation a single coupling constant was used for three different superexchange pathways mediated via $(\mu\text{-O})_2$ units, while the interactions through μ_2-alkoxo bridges are associated with singly bridged Fe units. However, for the interactions for which P was determined, the values of P and J are in good agreement with the correlation deduced by Gorun and Lippard. In addition, the J values determined for complexes **1**−**9** are generally in good agreement with literature values determined for corresponding binding modes in other ferric complexes. In particular, for exchange mediated by a single μ_2-alkoxo bridge, J varies from −8 to −13 cm^{-1}, which is consistent with the literature values of −6 to −26 cm^{-1}.[34] Moreover, the coupling constants determined for the $(\mu_2\text{-alkoxo})_2$ bridges for **1**·CH_2Cl_2 and **6**·H_2O of −7 to −11 cm^{-1} are consistent with the literature values of −4 to −27 cm^{-1}.[35] However, as mentioned above, the J values obtained for the interactions mediated by a $(\mu\text{-O})_2$ bridge for **7**, **8**·H_2O, and **9**·$2H_2O$ actually characterize the effect of three separate bridging units: one (μ_2-alkoxo)-(μ_3-hydroxo)(μ_2-carboxylato), one (μ_2-phenoxo)(μ_3-hydroxo), and one (μ_3-oxo)(μ_3-hydroxo). Thus, it is difficult to compare the determined J values with those from the literature or theory. The literature suggests that the values for the (μ_2-alkoxo)(μ_3-hydroxo)(μ_2-carboxylato) and (μ_2-phenoxo)-(μ_3-hydroxo) pathways should be similar, with previously observed values of −7 to −12 cm^{-1}.[35] Although examples of (μ-oxo)(μ-hydroxo) bridges are relatively rare, one family of ferric complexes with (μ_2-oxo)(μ_2-hydroxo) bridges is reported to have J values of −27 to −57 cm^{-1}.[30] Nevertheless, direct comparison of these species with the present complexes is difficult, due to the different metric parameters associated with the μ_3-bridging in **7**−**9** versus the μ_2-bridging observed for the literature species. It is not improbable that smaller J values will result from the longer Fe−O and Fe···Fe distances that occur in the μ_3 case. Finally, for **7**, **8**·H_2O, and **9**·$2H_2O$, the coupling constant associated with a single μ_3-oxo bridge is comparable to "body to wing" coupling constants of −30 to −50 cm^{-1} determined for Fe^{III}_4 "butterfly" complexes, which involve a similar bridging geometry.[41]

The magnetic susceptibility data for the bi-, tri-. and tetranuclear complexes can all be modeled satisfactorily without considering the effects of ZFS or intermolecular exchange interactions. However, for the pentanuclear complexes the rapid decrease in $\chi_M T$ as the temperature approaches zero is consistent with the presence of one or both of these phenomena. Although the structural and magnetic measurements were performed on differently solvated forms of these species, the structural data can give some insight into possible intermolecular interactions. Typically, intermolecular interactions are either propagated through a superexchange pathway involving intermolecular hydrogen bonds or arise from dipolar (through-space) interactions. Inspection of the structural data for **7**·H_2O·C_7H_8·$0.5C_6H_{14}$, **8**·$0.25H_2O$·$4.5CH_2Cl_2$, and **9**·$1.5H_2O$·$2CH_2Cl_2$·$0.5C_2H_4O$ indicates that there are no intermolecular hydrogen bonds that link Fe_5 units, and it seems unlikely that such bonds are present in **7**, **8**·H_2O, and **9**·$2H_2O$. In addition, the X-ray data reveal closest intermolecular Fe···Fe approaches of 7.1−7.2 Å for all three complexes, while closest centroid···centroid (where the centroid is arbitrarily defined as the center of the $(\mu\text{-O})_2$-bridged Fe_2 unit) distances are 11.5, 9.8, and 9.6 Å for **7**·H_2O·C_7H_8·$0.5C_6H_{14}$, **8**·$0.25H_2O$·$4.5CH_2Cl_2$, and **9**·$1.5H_2O$·$2CH_2Cl_2$·$0.5C_2H_4O$, respectively. Treating the complexes as point dipoles with $S = 5/2$ and using the mean field approximation

$$E_{dip} = \mu_0(gS\mu_B)^2/4\pi Vk_B \qquad (13)$$

where V is the molecular volume (1698 $Å^3$ for **8**·$0.25H_2O$·$4.5CH_2Cl_2$), the energy associated with the dipolar interactions (E_{dip}) is determined to be ∼0.01 cm^{-1}, which is essentially negligible. Furthermore, experimentally no evidence for strong intermolecular interactions is observed in the low-temperature micro-SQUID magnetization measure-

(40) Gorun, S. M.; Lippard, S. J. *Inorg. Chem.* **1991**, *30*, 1625.

(41) (a) McCusker, J. K.; Vincent, J. B.; Schmitt, E. A.; Mino, M. L.; Shin, K.; Coggin, D. K.; Hagen, P. M.; Huffman, J. C.; Christou, G.; Hendrickson, D. N. *J. Am. Chem. Soc.* **1991**, *113*, 3012. (b) Boudalis, A. K.; Lalioti, N.; Spyroulias, G. A.; Raptopoulou, C. P.; Terzis, A.; Bousseksou, A.; Tangoulis, V.; Tuchagues, J. P.; Perlepes, S. P. *Inorg. Chem.* **2002**, *41*, 6474 and references therein.

ments of **8**·0.25H_2O·4.5CH_2Cl_2, where a characteristic sigmoidal shape is often associated with antiferromagnetic intermolecular interactions.[18] Thus, it can be concluded that the three pentanuclear complexes do not possess intermolecular exchange interactions of a significant magnitude.

In the absence of intermolecular interactions, the rapid decrease in $\chi_M T$ as the temperature approaches zero for the pentanuclear complexes may be attributed to the effect of ZFS of the $S = 5/2$ ground state. In addition, the magnetization data can be modeled by considering an axial ZFS parameter D, with D values of ± 0.3 to ± 0.5 cm^{-1} determined for the three complexes. Low-temperature micro-SQUID measurements on **8**·0.25H_2O·4.5CH_2Cl_2 confirm the presence of an easy axis and therefore a negative D value. D values of similar sign and magnitude have been determined previously for other polynuclear ferric complexes.[8−13] The origin of these has been attributed to a combination of the effects of single-ion anisotropy of the Fe^{III} centers and spin−spin interactions. In particular, it has been suggested that a planar arrangement of the Fe centers in polynuclear ferric complexes (with axial symmetry and a non-zero spin ground state) is best suited to provide easy-axis-type magnetic anisotropy through spin−spin interactions.[10] This type of anisotropy is necessary for SMM behavior, and indeed most of the reported ferric SMMs do feature an essentially planar arrangement of the Fe atoms.[8−13]

The $S = 5/2$ and $D \approx -0.4$ cm^{-1} values suggest that the pentanuclear complexes should have an anisotropy barrier to magnetization reversal of $(S^2 - 1/4)|D| \approx 2.4$ cm^{-1}. Although this barrier is small, low-temperature micro-SQUID measurements on **8**·0.25H_2O·4.5CH_2Cl_2 reveal hysteresis at nonzero field, consistent with slow magnetization relaxation associated with a molecular anisotropy barrier. The faster time scale of Mössbauer spectroscopy allows for the observation of slow relaxation at temperatures higher than those associated with magnetic measurements. However, Mössbauer spectra of **8**·H_2O down to 1.7 K display no evidence of the magnetic splitting that would indicate such slow relaxation. It is probable that measurements at even lower temperatures are necessary to detect slow relaxation associated with such a small energy barrier.

An INS study of the trinuclear complex **2** was performed to gain additional insight into the magnetic behavior. The susceptibility data were fit assuming a single species and a scalene triangular arrangement of the Fe centers. However, from the INS data it was apparent that two distinct species were responsible for the observed behavior, and the data were modeled assuming two isomeric complexes, each with an isosceles triangular arrangement of the Fe centers. This is consistent with the observation of two independent molecules in the crystallographic asymmetric unit, which have different metric parameters (and enantiomeric configurations). The parameters derived from modeling the INS data afford a simulation of the susceptibility data that reproduces the experimental data extremely well (Figure 6a). This demonstrates the utility of the spectroscopic technique of INS in this situation, where the presence of two distinct complexes is clearly evident from the data. In contrast, magnetic susceptibility measurements are bulk measurements which can give no indication of the presence of multiple species and which allow only a determination of J values that represent an average of the values associated with the different complexes.

Conclusions

Although it has previously been little used in such a capacity, $Fe(O_2CMe)_2$ has provided a starting point for the synthesis of a whole new family of polynuclear complexes. Following reaction with some simple polydentate Schiff base proligands, oxidation by air, and, in some cases, reaction with additional carboxylic acids, nine new bi-, tri-, tetra-, and pentanuclear ferric complexes have been obtained. These complexes feature unusual structures and novel core topologies. The exclusively antiferromagnetic exchange interactions propagated through these iron−oxygen cores have afforded spin ground states of 1/2 and 5/2 for the tri- and pentanuclear ferric complexes, respectively. INS studies have allowed a thorough exploration of the magnetic behavior of one of the trinuclear complexes, confirming that the observed behavior arises from two distinct species. Low-temperature magnetic studies have revealed that the pentanuclear complexes possess a small energy barrier to magnetization reversal that results from the molecular anisotropy. Thus, these species represent new examples of ferric complexes with a nonplanar arrangement of Fe centers that display slow relaxation of the magnetization associated with an anisotropy-induced energy barrier of molecular origin.

Acknowledgment. This work was financially supported by the Swiss National Science Foundation. Stefan Ochsenbein and Roland Bircher are acknowledged for their assistance in collection of the INS data.

Supporting Information Available: X-ray crystallographic files in CIF format for **1**·CH_2Cl_2, **2**·CH_2Cl_2, **4**·CH_2Cl_2, **5**·0.5MeOH, **7**·H_2O·C_7H_8·0.5C_6H_{14}, **8**·0.25H_2O·4.5CH_2Cl_2, and **9**·1.5H_2O·2CH_2Cl_2·0.5C_2H_4O, tables of selected interatomic distances and angles for **1**·CH_2Cl_2, **2**·CH_2Cl_2, **4**·CH_2Cl_2, **5**·0.5MeOH, **7**·H_2O·C_7H_8·0.5C_6H_{14}, **8**·0.25H_2O·4.5CH_2Cl_2, and **9**·1.5H_2O·2CH_2Cl_2·0.5C_2H_4O, plots of (a) $\chi_M T$ and χ_M vs T and (b) $M(N\mu_B))^{-1}$ vs HT^{-1} for **4**, **7**, and **9**·2H_2O, and variable-temperature Mössbauer spectra for **4** and **7** (PDF). This material is available free of charge via the Internet at http://pubs.acs.org.

IC049600F